Quantitative two-photon flow cytometry—*in vitro* and *in vivo*

Cheng Frank Zhong
University of Michigan
Electrical Engineering and Computer Science Department
Center for Ultrafast Optical Science
2200 Bonisteel Boulevard
Ann Arbor, Michigan 48109-2099

Eric R. Tkaczyk
University of Michigan
Electrical Engineering and Computer Science Department
Center for Ultrafast Optical Science
2200 Bonisteel Boulevard
Ann Arbor, Michigan 48109-2099
and
University of Michigan
Michigan Nanotechnology Institute for Medicine and Biological Sciences
Ann Arbor, Michigan 48109-0648

Thommey Thomas
University of Michigan
Michigan Nanotechnology Institute for Medicine and Biological Sciences
Ann Arbor, Michigan 48109-0648

Jing Yong Ye
University of Michigan
Electrical Engineering and Computer Science Department
Center for Ultrafast Optical Science
2200 Bonisteel Boulevard
Ann Arbor, Michigan 48109-2099
and
University of Michigan
Michigan Nanotechnology Institute for Medicine and Biological Sciences
Ann Arbor, Michigan 48109-0648

Andrzej Myc
Anna U. Bielinska
Zhengyi Cao
Istvan Majoros
Balazs Keszler
James R. Baker Jr.
University of Michigan
Michigan Nanotechnology Institute for Medicine and Biological Sciences
Ann Arbor, Michigan 48109-0648

Theodore B. Norris
University of Michigan
Electrical Engineering and Computer Science Department
Center for Ultrafast Optical Science
2200 Bonisteel Boulevard
Ann Arbor, Michigan 48109-2099
and
University of Michigan
Michigan Nanotechnology Institute for Medicine and Biological Sciences
Ann Arbor, Michigan 48109-0648

Abstract. Flow cytometry is a powerful technique for quantitative characterization of fluorescence in cells. Quantitation is achieved by ensuring a high degree of uniformity in the optical excitation and detection, generally by using a highly controlled flow. Two-photon excitation has the advantages that it enables simultaneous excitation of multiple dyes and achieves a very high SNR through simplified filtering and fluorescence background reduction. We demonstrate that two-photon excitation in conjunction with a targeted multidye labeling strategy enables quantitative flow cytometry even under conditions of nonuniform flow, such as may be encountered in simple capillary flow or *in vivo*. By matching the excitation volume to the size of a cell, single-cell detection is ensured. Labeling cells with targeted nanoparticles containing multiple fluorophores enables normalization of the fluorescence signal and thus quantitative measurements under nonuniform excitation. Flow cytometry using two-photon excitation is demonstrated for detection and differentiation of particles and cells both *in vitro* in a glass capillary and *in vivo* in the blood stream of live mice. The technique also enables us to monitor the fluorescent dye labeling dynamics *in vivo*. In addition, we present a unique two-beam scanning method to conduct cell size measurement in nonuniform flow. [DOI: 10.1117/1.2931077]

Keywords: flows; multiphoton processes; cells; biology.

Paper 07417R received Oct. 4, 2007; revised manuscript received Jan. 24, 2008; accepted for publication Jan. 29, 2008; published online Jun. 20, 2008.

1 Introduction

Fluorescence sensing/imaging is a well-established technology in biological analysis and medical diagnostics. Fluorescence microscopy enables imaging of cellular dynamics *in vitro* and *in vivo* by labeling specific subcellular components with fluorescent dyes (or more recently, quantum dots or fluorescence protein). Flow cytometry does not provide image information, but instead measures the total fluorescence from each cell; large populations of cells can be studied, providing

Address all correspondence to Eric R. Tkaczyk, University of Michigan, Electrical Engineering and Computer Science Department, Center for Ultrafast Optical Science, 2200 Bonisteel Boulevard, Ann Arbor, Michigan 48109 2099; Tel: 734–763–0209 or 734–763–4875; Fax: 734–763–4876; E-mail: etkaczyk@umich.edu

1083-3668/2008/13(3)/034008/19/$25.00 © 2008 SPIE

quantitative information on many important biological processes (e.g., receptor expression, analysis of intracellular proteins, etc.). Whereas flow cytometry is the most accurate and well-defined technology for measuring properties of single cells, and appears to be mature technology, it has not yet reached its full capability. Despite a large body of literature on multiphoton microscopy,[1,2] there are only a few early articles considering the possibility of multiphoton flow cytometry.[3,4] We demonstrate here that remarkable quantitative measurements are possible when ratiometric measurements are used in two-photon flow cytometry. The major advantage of this technique over modified two-photon imaging[5] is the potential for high throughput to obtain large sets of data on cells in a short period of time, as is the case for conventional flow cytometry when compared to confocal microscopy.

In a conventional flow cytometer, cell samples are injected into the center of a liquid stream (air can be used alternatively), called the sheath fluid, which hydrodynamically focuses the cells singly to a point of detection with an accuracy of ± 1 μm or better.[6,7] As each cell passes through the excitation point, at which one or multiple laser beams are focused, each cell receives an identical amount of excitation from the laser(s). Fluorescence intensity of labeled cells corresponds to the uptake of the probe used,[8] and fluorescence gating can be used to differentiate different cell populations. The fluidics system plays an important role to ensure quantitative fluorescent measurement of single cells; however, the strict requirement on the fluid flow excludes flow cytometry from applications with nonuniform flow.

There are basically two reasons to conduct flow cytometry under nonuniform flow. One is to replace the bulky complex fluidics system with highly simplified low-cost ones. The recent advancement in microfabrication has made it possible to miniaturize the fluidic system to reduce the cost and reagent volume consumption;[9–12] however, most of the microchip flow cytometers still require sheath liquids (or air[13]) for hydrodynamic focusing. Consequently, a large volume of sheath liquid (or high-pressure gas for an air sheath) is required to process a very small amount of sample suspension. Although non-sheath-flow-based devices have been demonstrated for cell counting or sorting,[14,15] drawbacks, such as channel clogging by sample particles or slow detection rate, must be resolved to produce reliable flow cytometry systems. Therefore, the ability to conduct flow cytometry without requirements on the fluidics opens new possibilities for the development of a miniaturized and versatile system.

The other reason is to adapt cytometry to nonuniform flow is for *in vivo* applications in blood vessels. The major limitation of conventional flow cytometry is its invasiveness. To analyze cells in the circulatory system, blood samples must be extracted from the living body. The isolation of cells from their native environment and the subsequent sample-processing procedures not only introduce potential artifacts, but make it difficult to examine the same cell population over continuous time periods as well. Although other techniques, such as confocal or two-photon microscopy, are able to image fluorescently labeled cells *in vivo*, it remains a challenge to track a specific cell population within the blood stream for quantitative measurements.[16–20]

We recently demonstrated a novel flow cytometer, which realized single cell detection with two-photon excitation using a femtosecond near-IR (NIR) laser.[21–24] Exploiting the ability of a single NIR beam to probe multiple fluorophores with two-photon excitation, we were able to use this system to simultaneously enumerate two distinct populations of circulating cells in a mouse and compare their depletion dynamics.[25,26] We also showed that use of an extended cavity laser with a reduced repetition rate enables enhancement of the fluorescence signal.[27] In the investigation reported here, we emphasize the issues associated with performing cytometry under conditions of nonuniform flow, such as is found for *in vivo* cytometry, and we demonstrate a novel method for obtaining quantitative information in spite of the irregular flow. We take advantage of the nonlinear property of the multiphoton excitation process generated by a tightly focused NIR femtosecond laser beam. With the localized excitation volume that is equal to or smaller than a single cell (~ 10 μm), one can simply focus a NIR femtosecond laser beam into a simple fluid system, where a sheath flow is not required, to selectively detect single cells. As opposed to the uniform excitation in conventional flow cytometry, cells are excited nonuniformly as they flow through the excitation region at random positions and velocities. The nonuniform excitation results in a broad fluorescence intensity distribution for uniformly stained cells. Thus, the fluorescence signal level alone cannot be used as a parameter to differentiate single cells. To compensate for the nonuniform excitation, we propose a dual-dye staining method: labeling the cells with two different dyes, one of which is always fluorescent (the "trigger") on excitation by a laser beam, and the other fluoresces only when the cell function changes (the "reporter"). As a cell flows through the excitation region, the fluorescence signal from the "trigger" dye reflects the amount of excitation the cell receives, while the fluorescence signal from the "reporter" dye informs the changes in cell functions. Fluorescence signals from two dyes that emit at distinct wavelengths can be detected by two spectral channels and the ratio of the "reporter" over "trigger" can be used to quantitatively measure cellular parameters. As we demonstrate, quantitative two-channel ratiometric measurement can be achieved with multifunctional nanoparticles for targeting.

In addition, we present preliminary experimental results in the development of a novel two-beam two-photon flow cytometric technique for detection of cell aggregation, with great potential for real-time noninvasive *in vivo* detection of cell aggregation. In general, platelet, leukocyte, and red blood cell aggregation is involved in pathological processes such as radiation damage.[28] Cell aggregation is also found in atherosclerosis, chronic inflammation, and thrombosis, which are common defects in the circulatory system. In conventional flow cytomety, cell size is determined by the forward scattering signals. This method can not be applied to *in vivo* measurements due to the geometry of the detection system. Here, the cell size measurement is carried out by observing the time duration as the cell flows through the excitation focus and normalizing to the cell velocity. To measure the cell velocity, we split the excitation beam to have two separate foci aligned along the capillary flow direction (Fig. 1); the spot size is set to be smaller than the cell size. The velocity of each cell is obtained by measuring the time delay between the two excitation spots.

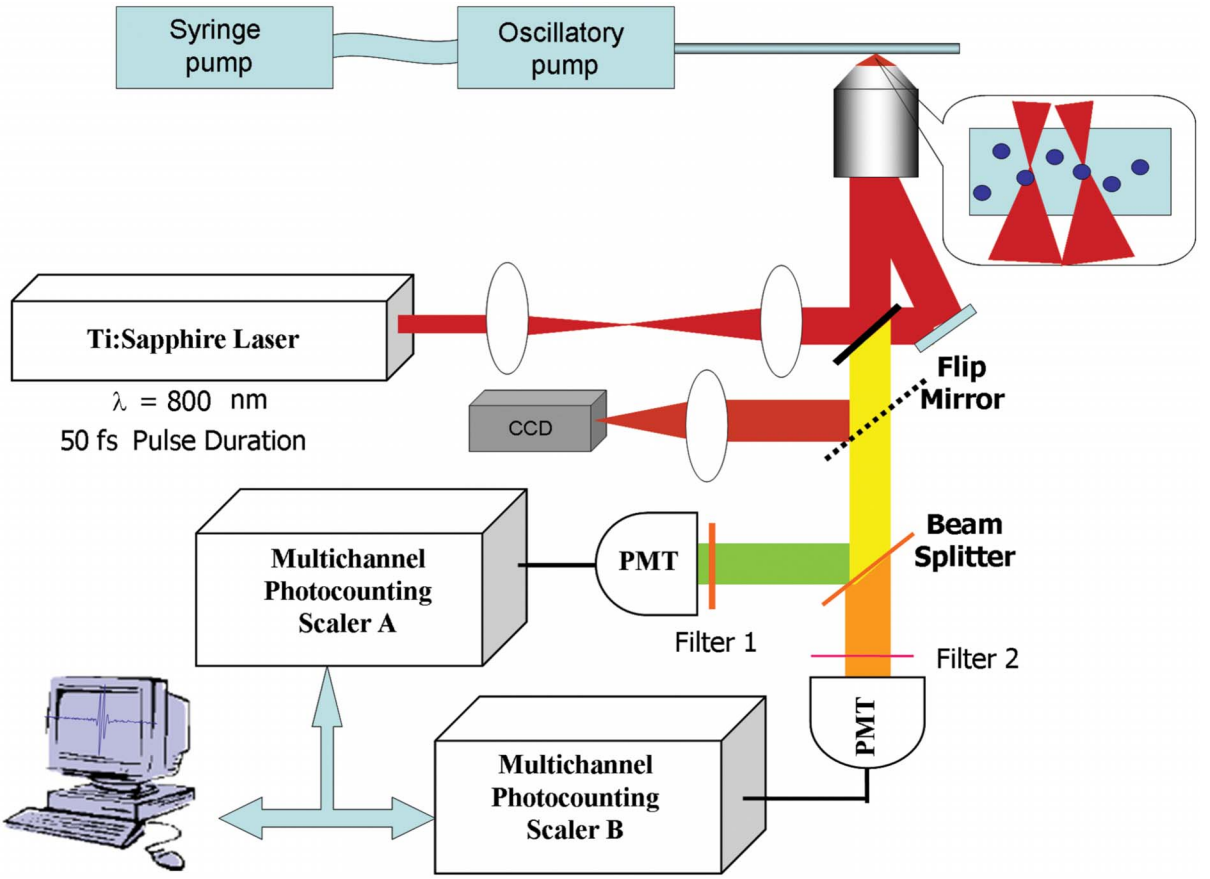

Fig. 1 Two-beam two-channel two-photon flow cytometry setup (T^3TC).

2 Instrumentation

A two-beam, two-channel and two-photon flow cytometer (T^3FC) was constructed (Fig. 1) to perform quantitative flow cytometry measurement under nonuniform flow both *in vitro* and *in vivo*.

2.1 *In Vitro Modeling Fluid System*

The *in vitro* modeling fluid system consisted of a square quartz capillary (Polymicro Technologies Inc.) and a fluid pump system. The square capillary (ID/OD: 100/300 μm) was prepared by burning away a 2-cm patch of the polyimide coating in the center of a 30-cm-long piece. The square capillary was held perpendicular to the excitation source with its surface adjusted flat to the source. The capillary was connected to a homemade oscillatory pump and a syringe pump (Fisher Scientific International, Inc., Hampton, New Hampshire) with plastic tubing. Cell samples were loaded into a syringe and pushed by the syringe pump through the capillary at constant flow rate (typically 5 μL/min). Pulsatile flow can also be superposed with a homemade oscillatory pump, which was described in detail previously.[21] The frequency and oscillation amplitude of the pulsatile flow pattern was obtained by analyzing sequencial images of a fluorescent microsphere flowing in the capillary. To model *in vivo* blood flow in the blood vessel of a mouse, the oscillation frequency was set to 11 Hz (typical mouse heart rate) and the oscillation amplitude was set to half of the average flow rate.

2.2 *Optical Setup*

The excitation source was a Ti:sapphire laser (Mira-900 Coherent Inc., Santa Clara, California), which generates 50-fs pulses at 800 nm with a 76-MHz repetition rate. For *in vitro* measurements, the *in vitro* modeling fluid system was used. The femtosecond laser pulses were focused by a long working distance Olympus 40×0.55 numerical aperture (NA)-microscope objective (Olympus America Inc., Melville, New York) into the square capillary tube (see the preceding fluid system). A telescope system was used to expand the laser beam to overfill the back lens of the objective, which produced a 2-μm spot in the focal plane. The point spread function (PSF) spreading has attracted much interest in multiphoton microscopy literature.[29,30] The PSF of the two-photon excitation system was measured by scanning a fluorescent microsphere (100 nm in diameter) at the focal plane of the objective and matched with theoretical calculation. The average excitation power used for cell measurements was between 10 and 20 mW at the focus. Group velocity dispersion from glass and mirrors was precompensated by a prism pair in the laser path. The femtosecond pulse width was adjusted to maximize the SHG (second-harmonic generated) signal from a BBO crystal, which was placed at the focal plane of the objective. The pulse width was further adjusted to maximize the fluorescence signal from dye solutions flowing in the capillary placed at the focal plane of the objective lens.

For single-channel or two-channel ratiometric measurement, the fluorescence from the excitation volume was collected back through the same microscope objective and separated from the excitation beam by a dichroic mirror. While we did observe very small, comparable to background scattering, SHG signals, the filter set in the system was chosen to prevent SHG and third-harmonic generated (THG) signals entering the detection channels. A long-pass filter in the excitation laser beam path cuts pump laser light leaking into the detection path, and a short-pass filter in the collection path further ensures collection of two-photon fluorescence only. Beamsplitters and bandpass filters were used to separate the fluorescence from different dyes into two channels, which were detected with two photomultiplier tubes (PMT HC7421-40, Hamamatsu Photonics, K.K., Hamamatsu City, Japan) and recorded with two multichannel photon-counting scalers (MCS SR430, Stanford Research Systems, Inc., Sunnyvale, California). The temporal bin width of the MCSs was set to correspond to the transit time of a cell through the excitation volume (typically 1.31 ms for a flow rate of 5 μL/min).

For two-beam scanning cell size measurement, the femtosecond laser pulses were split into two identical beams focused by the microscope objective into the capillary, with two distinct localized excitation region lined up along the fluid flow direction. The fluorescence signals from the two excitation regions were collected back through the same objective and sent to two identical channels, each detected with a PMT and recorded with a MCS. The temporal bin width of the MCSs was set to a much shorter time (typically 92 μs), so that the fluorescence signal from a single cell goes into several consecutive bins, which form a peak.

2.3 *Setup Modification for In Vivo Measurements*

For *in vivo* measurements, the *in vitro* modeling fluid system was replaced by a custom-made stage to hold anesthetized mice. An 8-mm-diam hole was drilled in the center of the stage, on top of which a glass slide was placed. The position of the mouse was adjusted to flatten one of its ears against the glass slide. The vasculature and blood flow of the mouse ear was visualized with a CCD camera by the Olympus 40× objective from transmitted light of a fiber optic illuminator (EW-41500-50, Cole-Parmer Instrument Company, Vernon Hills, Illinois). The femtosecond NIR laser beam was focused into the mouse ear with the objective from below. By switching off the short-pass filter in the fluorescence collection optical path, the back-scattered light from the femtosecond NIR laser beam was used to align the excitation beam to the blood vessel. The long focal length of the objective (5 mm) enabled the depth of the laser focus to be adjusted throughout the whole cross section of the mouse ear (less than 1 mm). To obtain a higher detection rate (probe a larger volume of blood) and reduce the autofluorescence background, the femtosecond NIR laser beam was adjusted to focus at the center of the blood vessel. The laser beam created an excitation region at the location where the blood flow speed is highest, while not generating autofluorescence from surrounding tissues. The aberration introduced by the highly scattering skin tissue made the size of the laser focus larger than 2 μm. The laser power after the objective was adjusted below 20 mW to avoid photodamage to either cells or tissue. The tissue at the focus of the femtosecond laser beam was periodically monitored with the same objective lens transilluminated by visible light. No obvious physical damage of the tissue was observed for the laser power we used.

3 Data Processing

A MATLAB (The Mathworks, Inc., Natick, Massachusetts) program was used to extract fluorescent peaks above the background noise level from the MCS trace signals. The background threshold in a detection channel was set at five standard deviations from the mean count rate of the background noise signal. The program scanned the trace signals for fluorescent peaks above the threshold. Once a peak was located, the peak characteristics, such as height (maximum fluorescent signal within the peak), width (number of consecutive bins above the background threshold) and location (the index of the maximum bin) were stored. For two-channel ratiometric measurements, two spectral channel traces were scanned simultaneously for peaks above their channel threshold level. For cell size measurement, the average and standard deviation of the transition time between the two excitation laser foci were first determined by cross-correlation of the two channel trace signals. The program scanned the two channel traces and fluorescent peaks above the threshold level were registered. Any two peaks (from different channels), separated by less than two standard deviations from the average transition time, were associated as a peak pair (fluorescent peaks from the same particle). For each peak pair, the number of bins above the threshold within the peaks (Δt) and the number of bins between the two peaks (T) were calculated. As the instant fluid flow speed is proportional to $1/T$, the transition time of a cell through a single focus (average of the two Δt) was normalized to the instant fluid speed as $\Delta t/T$, which is proportional to the cell size. For *in vivo* two-photon flow cytometry measurements, high frequency noise was removed from the MCS trace signal by using a triangle average filter. In the DeepRed dye solution tail vein injection experiment, the threshold level used to count the fluorescent peaks is determined by a small segment of the trace signal instead of using the whole trace.

4 Materials and Methods

4.1 *Computer Simulation*

A Monte Carlo simulation program of the two-photon excited flow cytomety system was written in MATLAB, which incorporated an accurate model of the two-photon excitation volume generated by a femtosecond NIR laser within a microcapillary. This program enables the user to set a wide variety of experimental parameters, including the laser beam characteristics, the flow rate and spatial distribution of simulated fluorescent particle within the capillary, the size and fluorescent dye distribution within particles, and white-noise levels.

To reveal the difference between one-photon and two-photon excitation, the axial direction of the laser beams (z axis) was set perpendicular to the fluid flow direction (x axis) and the coordinate was centered at the laser focal point. The program calculated the one-photon and two-photon excited fluorescence signal for grid points within the excitation volume ($100\times100\times100$ μm) at resolution of 20 nm and saved

the results as a lookup table. By integrating the grid points along the x axis, the fluorescence intensity distributions in the flow cross section of the fluid channel (y-z plan) were obtained.

To investigate the wide distribution induced by the inhomogeneous spatial distribution of dyes, two models representing different fluorescent dye distributions were used: (1) a uniformly distributed fluorescent sphere (10 μm in diameter) and (2) a fluorescent shell (10 μm in diameter). The fluorescent sphere was used as a model for fluorescent dye that evenly distributed in a cell, such as CFSE; while the fluorescent shell was used as the model for dye that only distributed with the cytoplasm of a cell, such as DeepRed. Using the two-photon excited fluorescence look-up table already described, the fluorescence signal from a 10-μm fluorescent sphere or shell was calculated for grid points within the excitation volume at a 100-nm resolution. Given the low Reynolds number (less than 10) of our flow cytometry system, it was assumed that the fluid flow was laminar and the fluorescent spheres or shells followed the fluid flow (x axis). The fluorescence intensity distribution of the fluorescent sphere or shell in the cross section of the fluid channel was determined by integrating the fluorescence along the fluid flow direction. By correlating the distribution of the 10-μm sphere and shell models, a two-channel dot plot was generated after normalization of the signal to unity in both channels.

4.2 *Fluorescent Microspheres*

Fluorescence microspheres with different size and spectral properties were obtained from Molecular Probes, Inc. (Eugene, Oregon). To calibrate the T^{3}FC system for cell size measurement, three types of fluorescence microspheres were used: A7302, AlignFlow flow cytometry alignment beads, 2.5 μm; A7303, AlignFlow Plus flow cytometry alignment beads, 6 μm; and F8836, FluoSpheres polystyrene microspheres, 10 μm. All three types of fluorescence microspheres have the same emission maximum at 515 nm. The diameter of each type of microspheres is uniform with a cell volume less than 4%. For sample preparation, all types of fluorescent microspheres were diluted in distilled water to a concentration of 3×10^5/mL. For *in vivo* flow cytomety measurements, F-8827 FluoSpheres® carboxylate-modified microspheres, 2.0 μm, yellow-green fluorescent (Ex505/Em515) was used.

4.3 *Cell Culture*

4.3.1 *Materials for cell labeling*

The 5-(and-6)-carboxyfluorescein diacetate, succinimidyl ester (CFSE), and MitoTracker® DeepRed 633 were purchased from Molecular Probes, Inc. (Eugene, Oregon). Trypsin-EDTA, Dulbecco's phosphate-buffered saline (PBS), fetal bovine serum (FBS), cell culture antibiotics, and RPMI media were obtained from Gibco/BRL (Gaithersburg, Maryland). The conjugates of PAMAM dendrimer with dyes were designed and synthesized at the Center for Biologic Nanotechnology (Ann Arbor, Michigan). The following conjugates were used: generation 5 dendrimer with DeepRed and folic acid (G5-DR-FA) and generation 5 dendrimer with FITC and folic acid (G5-FI-FA).

4.3.2 *CFSE-stained Jurkat and KB Cells*

Jurkat, an acute T cell leukemia cell line, clone E6-1 and KB, a human oral epidermoid carcinoma cell line were purchased from the ATCC (Manassas, Virginia, USA). Jurkat and KB cells were cultured in RPMI 1640 medium supplemented with penicillin (100 units/mL), streptomycin (100 μL/mL), and 10% heat-inactivated FBS. Prior to staining, the Jurkat and KB cells were washed in PBS and resuspended in PBS at concentration 10^6 cells/mL. To stain cells with CFSE, 500 nM (final concentration) of the dye was added to the cell suspension and cell were stained for 8 min at room temperature. After staining, the cells were washed three times with PBS supplemented with 2% FBS, resuspended in PBS and kept on ice until analyzed.

4.3.3 *CFSE- and DeepRed-stained PMBC*

Peripheral mononuclear blood cells (PMBCs) were isolated from the blood collected from 5-week-old, specific-pathogen-free female C3H/HeNHsd mice (Harlan, Indianapolis, Indiana) using Histopaque®-1077 (Sigma Diagnostics, Inc., St. Louis, Missouri). PMBC were cultured in RPMI 1640 medium supplemented with penicillin (100 units/mL), streptomycin (100 μL/mL), and 10% heat-inactivated FBS. Prior to staining, the PMBC were washed in PBS and resuspended in PBS at concentration 10^6 cells/mL. To stain cells with DeepRed, 500 nM (final concentration) of the dye was directly added to the cell suspension and cells were stained for 30 min at 37 °C. After staining, cells were washed three times with PBS. To stain cells with CFSE, 500 nM (final concentration) of the dye was added to the cell suspension and cell were stained for 8 min at room temperature. After staining, the cells were washed three times with PBS supplemented with 2% FBS, resuspended in PBS and kept on ice until analyzed.

4.3.4 *G5-FI-FA- and G5-DR-FA-labeled KB cells*

KB cells were maintained in folate-free medium containing 10% FBS as described before.[31] The KB cells were rinsed and incubated in folate- and serum-free medium with different concentrations of the G5-FI-FA and G5-DR-FA conjugates for 1 h at 37 °C. The treated cells were detached from their substrate with 0.25% trypsin, washed, and fixed with p-formaldehyde (to enable conventional flow cytometry follow-up the day after experimentation), then washed again and resuspended in PBS. A portion of the cells was analyzed by conventional flow cytometry. A second portion of the dendrimer-treated cells were analyzed by two-photon flow cytometry. For confocal microscopy, KB cells plated on glass cover slips were treated with a mixture 200 nM each of G5-FI-FA and G5-DR-FA for 3 h under conditions already described.

4.3.5 *Jurkat cell aggregates*

The Jurkat cells aggregates were obtained according to modified scaffolded receptor clusters method.[28] Briefly, CFSE-stained single cell suspension of Jurkat cells were incubated at 4 °C or RT with various concentrations (5 to 100 μM) of Concanavalin A (Sigma-Aldrich Co. St. Louis, Missouri), which crosslinks mannose glycoproteins on the cell surface, in HBS-Ca^{+2} buffer. After 30-min to 1-h incubation, cells were gently centrifuged at 500 rpm, the Concanavalin A so-

Table 1 Concentration of dye conjugates used to incubate KB cell samples and their mean channel fluorescence measured with a conventional single photon flow cytometer; for details, see treatment of KB cells with G5-FI-FA and G5-DR-FA in Sec. 4.

Sample No.	G5-FI-FA (nM)	G5-DR-FA (nM)	G5-FI (nM)	G5-DR (nM)	Mean Channel Fluorescence	
					FITC (a.u.)	DeepRed (a.u.)
1	200	0	0	0	95.8	5.3
2	180	20	0	0	77.8	325.2
3	150	50	0	0	60.8	837.8
4	120	80	0	0	44.7	1138.3
5	80	120	0	0	42.7	2518.3
6	50	150	0	0	20.4	2141.3
7	20	180	0	0	9.7	2372.3
8	0	200	0	0	3.5	2365.8
9	0	0	0	0	2.86	5.86
10	0	0	200	0	3.4	5.1
11	0	0	0	200	2.9	12.2

lution was removed, and cells were resuspended 3 mL of cold HBS-Ca^{+2}. The induced aggregation was confirmed under a microscope.

4.3.6 *CFSE or DeepRed labeled splenocytes for in vivo FC*

Spleens were collected from euthanized animals and were disrupted in PBS to obtain a single cell suspension after which the cells were washed in PBS and the red blood cells were lysed using ammonium chloride. To stain the splenocytes with CFSE, the cells were resuspended in PBS and stained with 500 nM CFSE for 8 min at room temperature. After staining, cells were washed with PBS containing 2% FBS. To stain the splenocytes with DeepRed, the cells were treated with DeepRed, incubated for 1 h at 37°C, trypsinized, rinsed, and resuspended in PBS, pH 8.

4.4 *Confocal Imaging of Cells*

Confocal images of PMBC stained with both CFSE and DeepRed, KB cells stained with both G5-FI-FA and G5-DR-FA were acquired using an Olympus Confocal Microscope (Olympus America Inc., Melville, New York). The cells were rinsed, fixed with paraformaldehyde, and mounted on a slide and confocal images were taken in an Olympus Confocal Microscope. An argon laser was used to excite CFSE or FITC and the fluorescent signal was recorded in the green channel; while a He/Ne laser was used to excite DeepRed and the signal was recorded in the red channel. The green and red channel images of the PMBC stained with CFSE and DeepRed were combined to form a single image [Fig. 5(a) in Sec. 5]; while KB cells stained with both G5-FI-FA and G5-DR-FA images were separately shown in green [Fig. 5(b) in Sec. 5] and red channel [Fig. 5(c) in Sec. 5].

4.5 *Conventional Flow Cytometry Analysis*

4.5.1 *CFSE and DeepRed labeled PMBC*

A portion of the CFSE- and DeepRed-labeled PMBC was analyzed by conventional flow cytometry in an Aria flow cytometer (Becton Dickinson, Franklin Lakes, New Jersey) using excitation and emission wavelengths specific for the two dyes. The viable cells were gated, and the mean FL1-fluorescence of 10,000 cells was acquired. The result showed the saturation of the dye uptake in both CFSE and DeepRed channels.

4.5.2 *G5-FI-FA and G5-DR-FA labeled KB cells*

A portion of the G5-FI-FA and G5-DR-FA labeled KB cells was analyzed by conventional flow cytometry in a FACScan flow cytometer (Becton Dickinson, Franklin Lakes, New Jersey) using excitation and emission wavelengths specific for the two dyes. The viable cells were gated, and the mean FL1-fluorescence of 10,000 cells was quantified. Conventional flow cytometry showed binding of the two dendrimers in proportion to the concentration of the individual dendrimer used in the mixture (Table 1).

4.5.3 *Circulating fluorescent microspheres and CFSE-labeled splenocytes*

The 2-μm, yellow-green fluorescent (Ex505/Em515) microspheres were washed, resuspended in 200 μL of PBS (total number of beads 2.3×10^9), and injected via tail vein to CD-1

mice. Spleens were collected from euthanized animals and were disrupted in PBS to obtain a single cell suspension after which the cells were washed in PBS and the red blood cells were lysed using ammonium chloride. Splenocytes were resuspended in PBS and stained with 5 μM CFSE dye for 8 min at room temperature. After staining, cells were washed with PBS containing 2% FBS and 3.6×10^6 splenocytes in 200 μL PBS were injected via tail vein to NU/NU CD-1 mice.

Blood samples were obtained either from the tail vein or from euthanized premorbid animals by cardiac puncture at different time intervals during the course of the experiment. Blood was collected to heparinized tubes and diluted 10 times with PBS prior to flow cytometry analysis. Samples were acquired on a Coulter EPICS-XL MCL Beckman-Coulter flow cytometer and data were analyzed using Expo32 software (Beckman-Coulter, Miami, Florida).

4.6 *Animals*

Five- to six-week-old, specific-pathogen-free female NU/NU CD-1 and CD-1 mice were purchased from Charles River Laboratories (Portage, Michigan) and housed in a specific pathogen-free animal facility at the University of Michigan Medical Center in accordance with the regulations of the University's Committee on the Use and Care of Animals as well as with federal guidelines, including the principles of Laboratory Animal Care. CD-1 mice were used for the fluorescent microsphere-circulation *in vivo* experiments. Immmunodeficient, NU/NU CD-1 mice were used for DeepRed-labeled cell circulation and free DeepRed dye injection *in vivo* experiments. All injections were performed via the tail vein.

4.7 *In Vivo Two-Photon Flow Cytometry Measurements*

To conduct *in vivo* two-photon flow cytometry (IVTPFC) measurements, mice were anesthetized by inhalation of isoflurane. The mice were placed on the T^3FC stage with one ear taped to the glass slide window for optical detection. A blood vessel roughly 50 μm in diameter with ample blood flow was selected for cytometry measurement. Depending on the anesthesia condition, the mice may breathe heavily during the data acquisition, which induces movement of its ear. This tremble can be easily seen with the transilluminated microscopy image. The alignment of the laser focus and the blood vessel within the mouse ear was checked before and after each data acquisition to be within a few micrometers. Before injection of the solution of fluorescent-dye-labeled microspheres or cells, the background signals in both the S channel and the L channel were recorded as a control. The laser power used was below 20 mW and no photodamage to the ear of the mice was observed after the experiments.

To monitor circulating fluorescent microspheres *in vivo*, 200 μL sodium chloride solution containing 2.3×109 yellow-green fluorescent (Ex505/Em515) 2.0-μm microspheres was injected into CD-1 mice through tail vein. Immediately following the injection, the two-channel fluorescence signals from a blood vessel were recorded. The same amount of microspheres was injected through the tail vein 11 min after the initial injection.

To monitor circulating DeepRed-labeled fluorescent cells *in vivo*, 300 μL PBS containing 3.6×10^6 DeepRed-labeled splenocytes was injected into NU/NU CD-1 mouse initially with additional injection of the same dose 25 min after. The two-channel fluorescence signal was recorded immediately after each injection and repeated at the same vessel location roughly 2 h and 1 day after the initial injection.

To monitor the fluorescence from free dye *in vivo*, 300 μL DeepRed dye solution (5 μM) was injected into NU/NU CD-1 mouse through tail vein. The fluorescence was acquired in two channels immediately following the injection and repeated at the same vessel location roughly one and half hours after.

5 Results and Discussion

5.1 *Single-Cell Detection Using a Femtosecond Laser*

Using the flow cytometry simulation program (details in Sec. 4), we ran two simulations of the fluorescence excitation distribution in the cross section of a fluid channel for one-photon [Fig. 2(a)] and two-photon excitation [Fig. 2(b)]. For comparison, 400- and 800-nm laser beams with a 2-μm waist at the focal plane were used. As shown in Fig. 2(a), in the case of one-photon excitation, the laser beam excites all the fluorescent dyes along its optical path, creating a broad excitation region within a fluid stream. Under nonuniform flow conditions, such as *in vivo* capillary blood flow, multiple cells may enter the excitation region simultaneously. Thus, single-cell detection may not be achieved, unless a confocal pinhole is used to restrict the detection region to the focus.[36] In the case of two-photon excitation, however, the probe volume is confined to the laser beam focus, where the photon flux is highest. One can simply focus a femtosecond NIR laser beam into a fluid stream to create an excitation volume (a 0.5 NA objective creates an excitation region about 1 μm laterally and 5 μm longitudinally) equal to or smaller than a cell, so that only one cell enters the localized excitation volume to be selectively detected.

For proof of principle, Jurkat cells labeled with CFSE and unstained Jurkat cells as a control were tested in our T^3FC system with a single detection channel. A short segment of the raw data is presented in Fig. 3(a). The horizontal axis denotes time and the vertical axis denotes fluorescence signal. Sharp peaks in the raw data correspond to bursts of photons emitted by single fluorescence-stained cells as they transit through the excitation beam. With identical excitation power, almost no fluorescence peak was observed above the background for the unstained Jurkat cells, while thousands of events were detected from CFSE-labeled Jurkat cells within a few minutes. Although the cells were uniformly stained (confirmed by flow cytometry data not shown here), the intensity distribution of the fluorescent signal from each cell spreads out from just above the background to the maximum possible signal level [Fig. 3(b)]. This is due to the fact that each cell enters the excitation region at a random position and speed. Depending on the amount of excitation received, the fluorescence signal from each cell peaks at a different intensity level. Due to the uneven excitation under two-photon excitation, the fluorescence intensity in a single channel itself cannot be used as a parameter to quantify cellular properties as in conventional flow cytometry. Nevertheless, our data clearly demonstrated

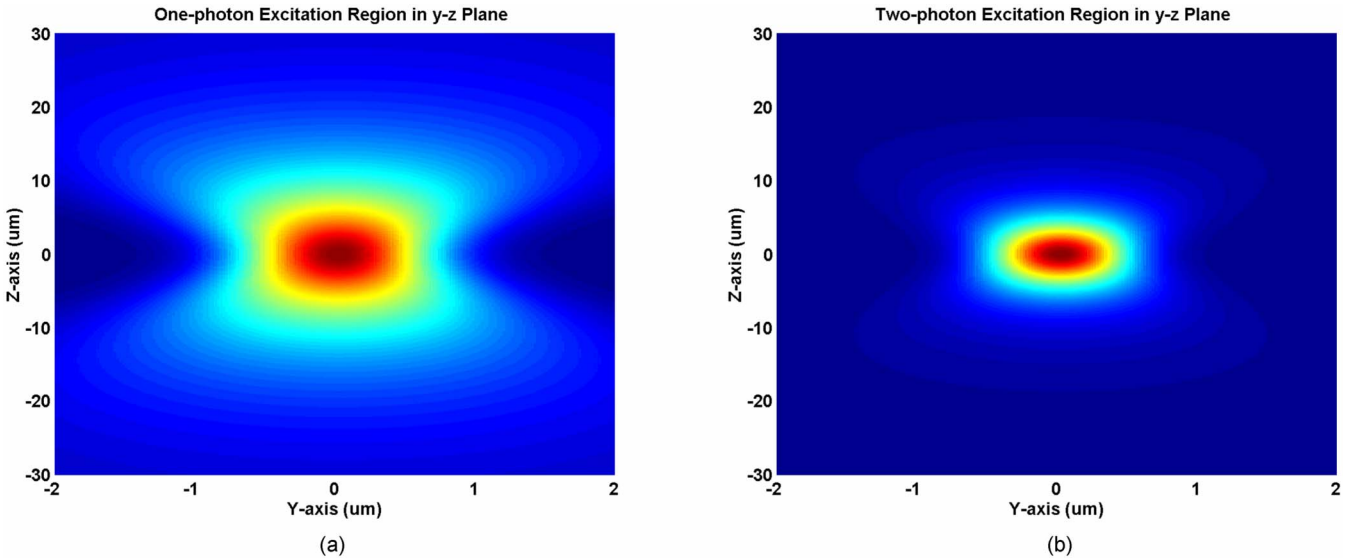

Fig. 2 Fluorescence intensity distribution of (a) one-photon and (b) two-photon excitation in the cross section of a flow channel. For comparison, both simulation results are based on a 800-nm laser beam with a 2-μm waist. The fluid flow direction is along the *X* axis, the laser beam propagates along the *Z* axis and centers at zero of the coordinates.

single-cell detection in nonuniform flow condition can be achieved under two-photon excitation.

5.2 *Quantitative Two-Channel Ratiometric Measurement*

To understand the condition for signal quantification using trigger and reporter dyes, mouse PMBCs stained with CFSE and DeepRed (details in Sec. 4) were investigated using the T^{3}FC system. The two-photon excited fluorescence signal has a wide distribution in the two-channel dot plot [Fig. 4(a)]. The fluorescence was filtered such that the short-wavelength detection channel (S channel) corresponds only to CFSE, and the long-wavelength channel (L channel) only to DeepRed. The wide distribution indicates the S channel signal was not correlated to the L channel signal, although saturation of the dye uptake (confirmed by conventional flow cytometry result) should yield such correlation. To examine the lack of correlation between the two channel signals, the dual-dye-stained PMBC was studied under a confocal microscope. The image shows that CFSE and DeepRed had different distributions within each cell [Fig. 5(a)]. The green nuclei and yellow cytoplasm of the cell indicate that CFSE was uniformly distributed through out the whole cell and DeepRed is located only in the outer cytoplasm surrounding the nucleus (DeepRed is a cell-permeating probe that binds to the outer membrane of mitochondria). To model the staining condition using the computer simulation program, 10-μm fluorescent spheres and shells were used to represent CFSE and DeepRed, respectively. The computer simulated cross sectional fluorescence distribution of the sphere [Fig. 4(c)] and the shell [Fig. 4(d)] do not match, which is due to the inhomogeneous localization of these two dyes within each bead. The unmatched distribution in the cross section of the fluid stream produces a wide distribution in a two-channel dot plot [Fig. 4(b)], which matches the result of the dual-dye-stained PMBC [Fig. 4(a)]. Thus, we can conclude that the different spatial localization of the two dyes within each cell leads to the lack of correlation between two channel signals under uneven excitation generated by the femtosecond NIR laser beam.

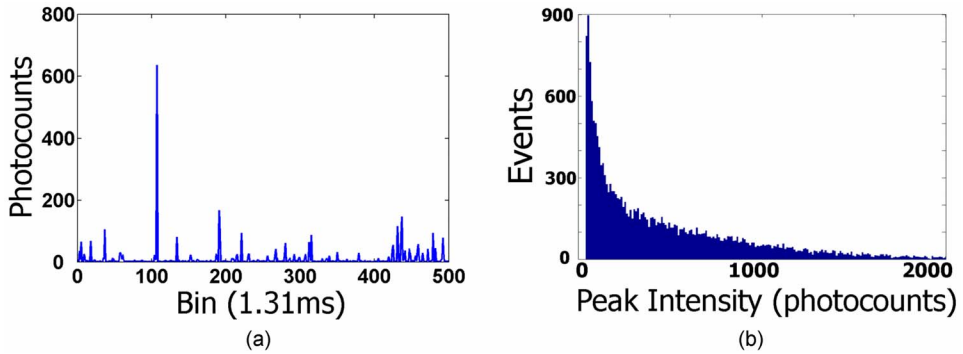

Fig. 3 Single-channel signal from T^{3}FC: (a) raw data, where each peak corresponds to a labeled cell passing through the laser focus, and (b) histogram of the intensity distribution of peaks in a single channel.

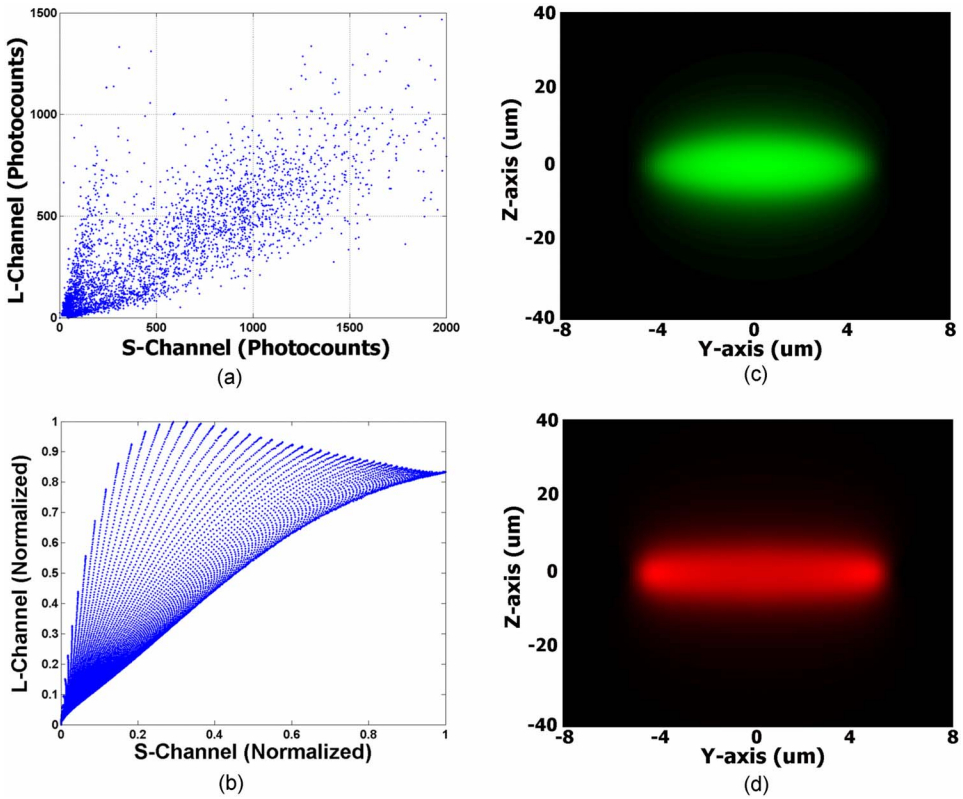

Fig. 4 Computer simulation result matches with experimental data: (a) two-channel dot plot of PMBCs stained with CFSE and DeepRed, where the two-photon excited fluorescent signals from CFSE and DeepRed go to S channel (green) and L channel (red), respectively; (b) computer simulated two-channel dot plot of dual-dye-stained microspheres; (c) fluorescence intensity distribution of a green-dye-stained 10-μm sphere in the cross section of the flow channel; and (d) Fluorescence intensity distribution of red-dye-stained 10-μm shell model in the cross section of the flow channel. The fluid flow direction is along the *X* axis, and the laser beam propagates along the *Z* axis and centers at zero of the coordinates. The *Y-Z* plane represents the cross section of the flow channel. The two-photon fluorescence signal from a sphere or shell is calculated as it centers at each point in the *Y-Z* plane. The dye in the sphere model is evenly distributed in the whole volume of a 10-μm sphere, while the dye in the shell model is evenly distributed on the surface of the same 10-μm sphere. The computer simulated dual-dye-stained 10-μm microspheres are the overlap of the sphere and shell model. The fluorescent signals from the sphere and shell go to the S and L channels, respectively. (Color online only).

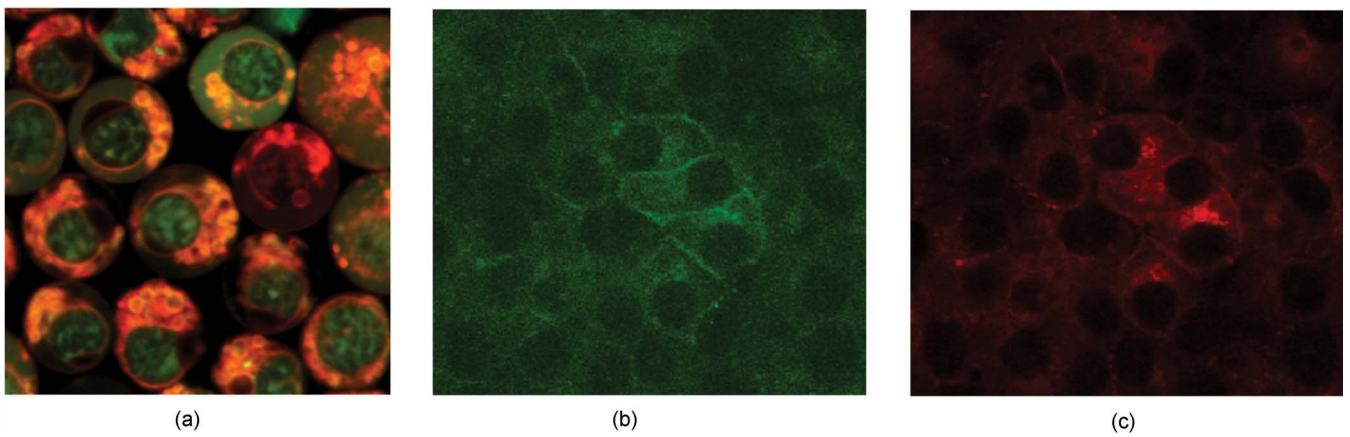

Fig. 5 Confocal microscopy images of (a) PMBC stained with CFSE (green) and DeepRed (red), (b) green channel of KB cells stained with G5-FI-FA and G5-DR-FA, and (c) Red channel of KB cells stained with G5-FI-FA and G5-DR-FA. The details are given in Sec. 4. (Color online only.)

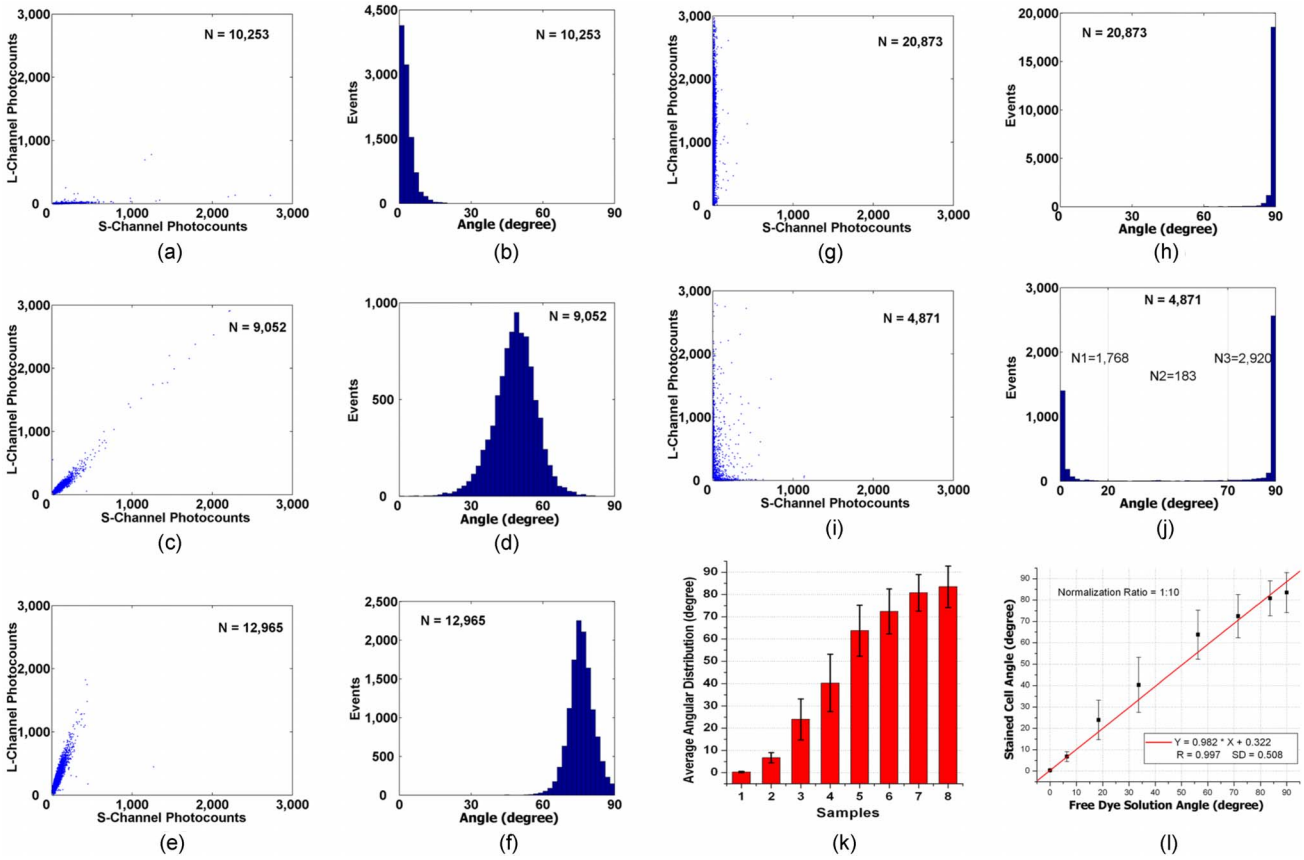

Fig. 6 Two-channel dot plot and angular distribution of KB cell samples stained with G5-FI-FA and G5-DR-FA at different concentrations. (a) and (b) Two-channel dot plot and angular distribution histogram from sample 1; (c) and (d) from sample 2; (e) and (f) from sample 3; (g) and (h) from sample 8; (i) and (j) from the mixture of sample 1 and sample 8 at a volume ratio of 1:1; (k) the average angular distribution of cell samples from 1 to 8; and (l) the average angle of KB cells stained with G5-FI-FA and G5-DR-FA at certain concentration ratio fits linearly to the ideal average angle of free G5-FI-FA and G5-DR-FA solutions used to incubate the KB cells. The concentration of dye conjugates used to incubate the KB cell samples are listed in Table 1.

To make quantitative ratiometric measurements, it is essential that the fluorescence amplitudes of signal and reporter be correlated (i.e., spatially correlated fluorescent labels must be used to enable a narrow angular distribution). One solution to establish the required correlation between the trigger and reporter dyes is to use targeted fluorochromes. For example, two dyes could be conjugated onto a nanoparticle, which is taken up into the cells via specific receptors. Alternatively, the dye molecules may be linked separately onto nanoparticles that have the same targeting agent. By competing for the same receptors, the dye concentrations in the cell become correlated. Specifically, the KB cell, which is an epidermoid carcinoma cell line known to express the receptor for folic acid (FA), was selected as a model for proof of concept. The nanoparticles used to carry the FA-targeting agent and fluorescent molecules are PAMAM dendrimers. Our previous studies have shown that KB cells bind and internalize FA-conjugated dendrimers in a receptor-mediated fashion.[31] Regardless of the dye molecules conjugated on the dendrimers, the FA on each of the dendrimers guides the PAMAM dendrimers to the FA receptor within the KB cells. This is confirmed with the identical structure in green [Fig. 5(b)] and red [Fig. 5(c)] channel confocal microscopy images. KB cells treated with the G5-FI-FA and G5-DR-FA at different concentrations (Table 1) were analyzed by the T^{3}FC. The FITC (FI) and DeepRed (DR) dyes correspond to the S and L channels, respectively. On a two-parameter dot plot (S channel versus L channel); the KB cells fall into well-separated clusters of narrow angular distribution [Fig. 6(a) to 6(h)] according to the variation on the concentrations of G5-FI-FA and G5-DR-FA. This enables one to differentiate a single-cell event in a mixed sample. With a mixture of KB cell samples under different incubation conditions through our capillary system, signals from different samples remain in the corresponding angular distributions [Figs. 6(i) and 6(j)]. Due to the different fluorescence quantum yield and two-photon excitation cross section of FITC and DeepRed, the number of photons detected in the L channel (sample 8) is roughly 10 times of the number detected in the S channel (sample 1). Taking the intensity difference into account, the average angular distributions of samples were normalized accordingly. As shown in Fig. 6(k), the average angular distribution increases with decreasing concentration ratio of G5-FI-FA to G5-DR-FA. The ideal angular distributions of different samples, assuming the uptake load of the nanoparticle is proportional to its incubation concentration, shows a linear fit with the experimental results [Fig. 6(l)]. Thus, the uptake of the dendrimer-dye-FA conju-

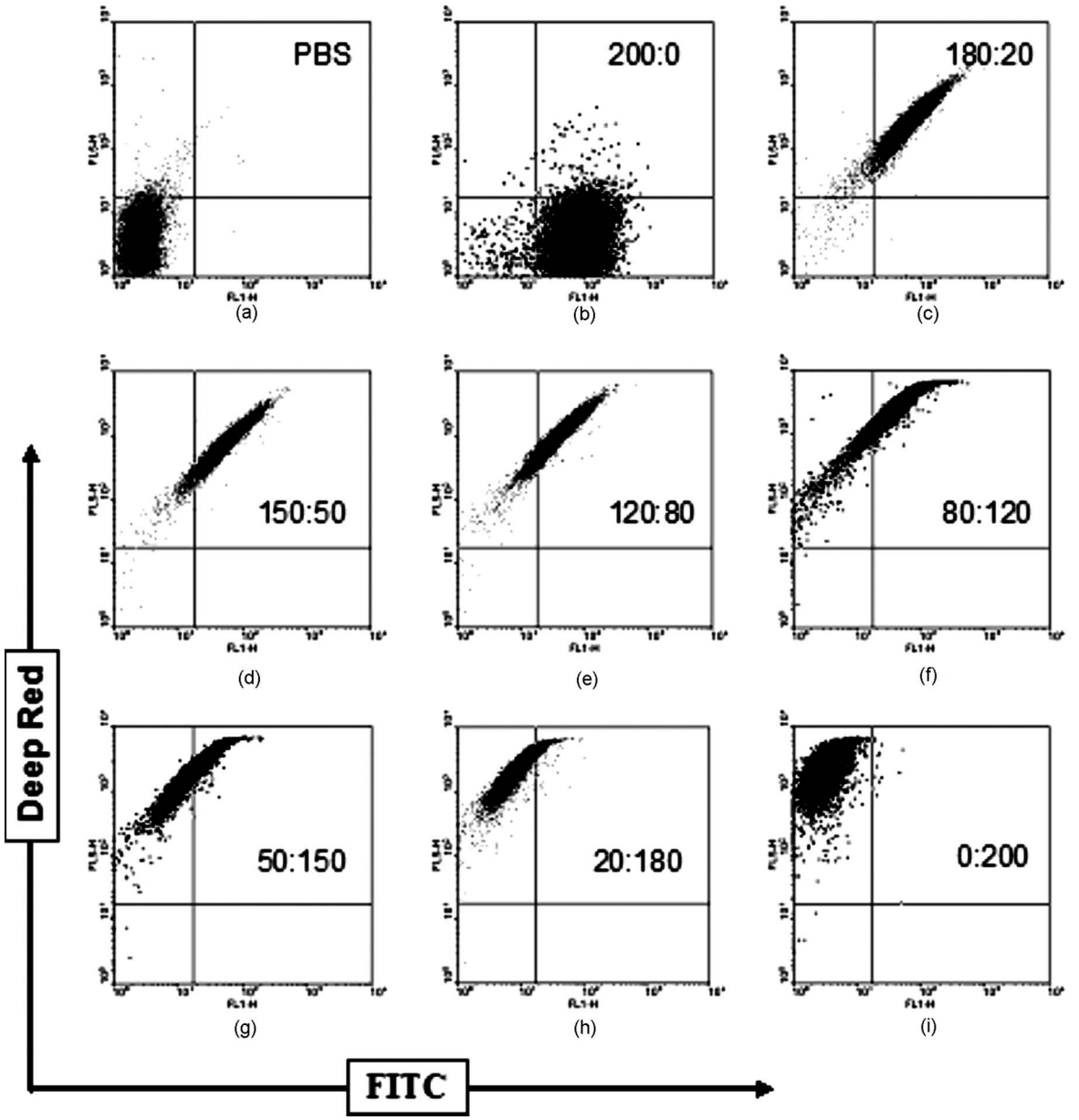

Fig. 7 Conventional flow cytometry of KB cells treated with different concentrations of G5-FI-FA and G5-DR-FA (the respective concentrations used are indicated), as described in Sec. 4: (a) unstained control in PBS; (b) to (i) correspond to samples 1 to 8 shown in Table 1, with the *X* and *Y* axes respectively representing the FITC and DeepRed fluorescence on a log scale. In the FITC channel, the mean channel fluorescence from sample 1 is set as 100%; in the DeepRed channel, sample 8 is set as 100%.

gates is proportional to the concentration of the dye-conjugated nanoparticles during cell incubation. This result is confirmed by conventional flow cytometry (Fig. 7). Conventional flow cytometry results [Fig. 7(a)] showed that the detected fluorescent signals (mainlyautofluorescence) for unstained KB cells (sample 9) and KB cells stained with nontargeted dendrimer-dye conjugates (samples 10 and 11) in both channels were much lower than those for KB cells stained with dendrimer-dye-FA conjugates. This was also observed by the T^3FC, where the number of cells detected was three orders of magnitude lower with the same background threshold.

The two-channel ratiometric method can be used to quantitatively measure the uptake of fluorescence-labeled-nanoparticles under nonuniform flow condition. If the fluorescence signal from one of the dye-conjugated nanoparticles is associated with cellular function, such as apoptosis, the ratiometric method can be used to quantitatively measure the cellular function. Furthermore, the ratiometric method is not limited to the dual dye staining scheme; the T^3FC can detect spectral shift or change from a single cell. One could envision further developing the system to perform fluorescence resonance energy transfer (FRET) measurements.

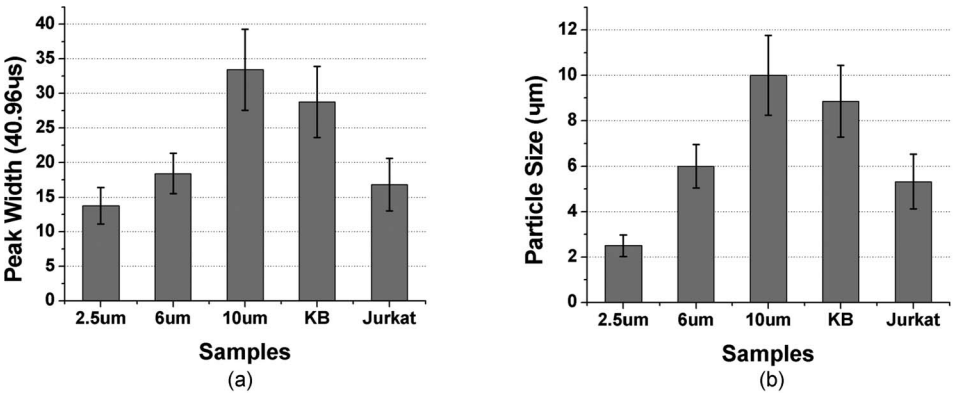

Fig. 8 Size measurements made using T^{3}FC: (a) average peak width (normalized duration time of cell passing through one excitation volume) of different samples, where the 2.5-, 6-, and 10-μm bars are the nominal diameter of fluorescent microspheres; KB stands for CFSE-stained KB cells and Jurkat stands for CFSE-stained Jurkat cells; and (b) actual particle size of the samples after deconvolution.

5.3 *Two-Beam Scanning Cell Size Measurement*

Light scattering is the standard method for determining cell size in flow cytometry. However, under nonuniform flow, this does not work (especially *in vivo*). Here, we conduct cell size measurement based on the fluorescence peak width normalized to flow velocity. By setting the temporal bin width of the MCSs to a much shorter time, a time-resolved fluorescence peak from 2.5-, 6-, and 10-μm fluorescent microspheres, CFSE-stained KB cells, and CFSE-stained Jurkat cells were obtained using the T^{3}FC. The fluorescence peak width was normalized to the flow velocity, inversely proportional to the transition time between two foci. The average peak width of each sample is shown in Fig. 8(a). As the average peak width is a convolution measure of the particle and the laser beam, it is not directly proportional to the size of the particle. A deconvolution function, which converts average peak width to average particle size, was determined using the fluorescent microspheres as calibration. The deconvoluted size of the samples is shown in Fig. 8(b). The size information obtained this way is a measure of the distribution volume of the fluorescent dye within a cell or particle, rather than the actual physical size of the cell or particle. With partial distribution of CFSE within cells, the two-beam scanning results may not reflect the actual size of KB cells or Jurkat cells. Further, cell clipping, where only a portion of the cell passes through the laser focus, is another potential source of artifacts not overcome by the normalization.

In addition to the cell size measurement, the T^{3}FC is also capable of cell aggregation detection. Time-resolved fluorescent peaks from CFSE-stained single Jurkat cell suspension and Jurkat cell aggregates were obtained in the T^{3}FC. Typical fluorescence peak profiles from the single-channel raw data are shown in Fig. 9. The peak width (number of bins above the background) of an aggregated Jurkat cell (103 bins) is much wider than that of a single cell (18 bins). The pulsatile flow generation device was used to further demonstrate the two-beam method in highly nonuniform flow. Suspensions of 6-μm fluorescent microspheres were analyzed using single-beam and two-beam scanning. Under the two-beam scanning scheme, the normalized peak width distribution of the florescent microspheres [Fig. 10(b)] is much narrower compared with the distribution using a single beam [Fig. 10(a)]. Considering the small standard deviation of the fluorescent microspheres (less than 4%), the normalized peak width should have a narrower distribution than what is shown in Fig. 10(b). The broadened peak width distribution is due to the random of each fluorescent microsphere in the excitation region (2 μm lateral); resulting different portion of each microsphere is scanned by the laser beam. We have shown previously that identical fluorescent microspheres produce different peak widths if they enter the excitation region at identical speed but different position relative to the laser beam.[21]

Although the two-beam scanning method does not offer absolute size measurement of single particles or cells, it grants sufficient accuracy to detect cell aggregation. To demonstrate the ability to detect cell aggregation in nonuniform flow, suspensions of 6 and 10 μm fluorescence microspheres were flown in the T^{3}FC. With two-beam scanning, the normalized peak width distribution of 6- and 10-μm fluorescence microspheres is shown in Figs. 11(a) and 11(b), respectively. Setting the differential threshold as 21 bins (dashed line), 2.9 and 95% of 6- and 10-μm fluorescence microspheres were above this level, respectively. This clearly demonstrates that the two-

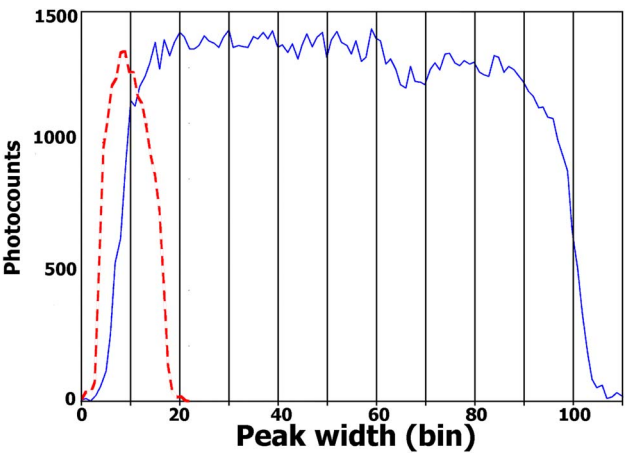

Fig. 9 Representative single-cell and aggregated Jurkat cell fluorescent profiles. The peak from a single Jurkat cell (dashed line) is much smaller than that of a cell aggregate (solid line). Each bin corresponds to 92 μs.

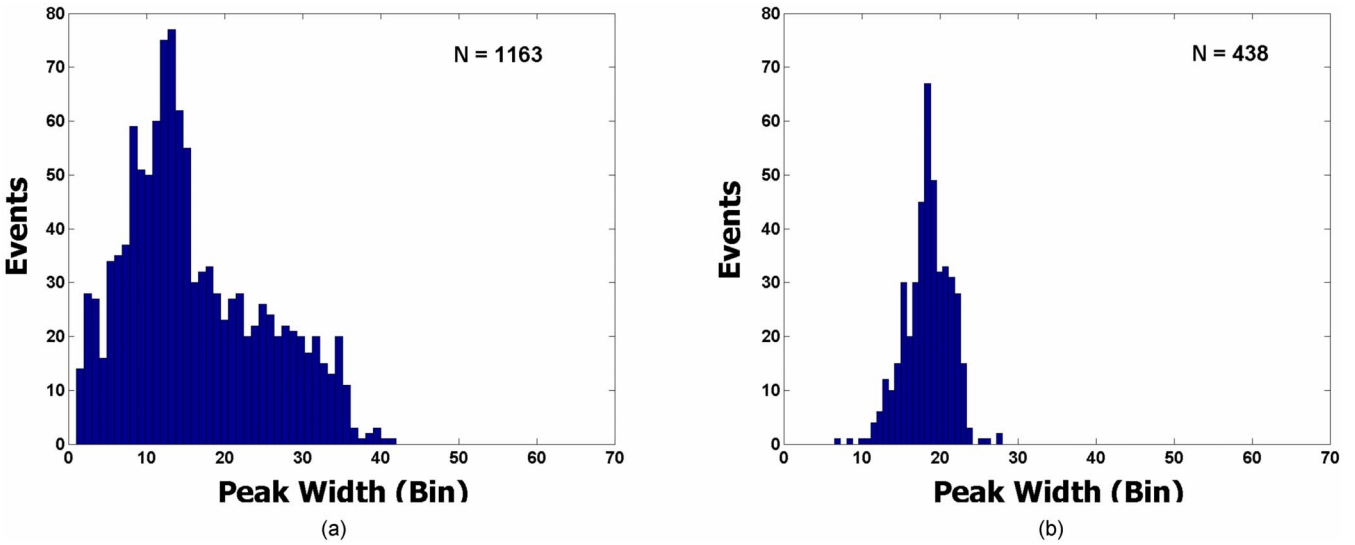

Fig. 10 Peak width distribution of 6-μm fluorescent microspheres (a) using the single beam setup and (b) using two-beam normalization.

beam scanning method is capable of identifying size differences under nonuniform flow conditions. For the aggregated (induced by ConA) Jurkat cells, 12.3% were above the threshold level [Fig. 11(d)], compared to 5.6% for the control cells [Fig. 11(c)]. As stated, the fluorescence peak width depends on the relative position of the particle in the excitation region. Similarly, the fluorescence peak width also relies on the orientation of aggregated cell cluster in the laser beam. Thus, the percentage difference between the aggregated and control sample may not reflect the actual difference in these samples. In spite of this, the results show that aggregation of Jurkat cells is reflected in the measurements under nonuniform flow condition.

A limitation of applying the two-beam method to *in vivo* measurements is that it can not differentiate events from a single cell passing sequentially through the two foci from two different cells passing through each of the focus. This technique is more suitable for cell size characterization under controlled flow, in which the flow speed is maintained constant and cell trajectory is limited by a small capillary. For *in vivo* blood flow conditions, such as stoppage or backward flow, this method may not work. For *in vivo* application under slower velocities, the cell concentration must be kept low to ensure that a cell passes through two foci before the next one arrives.

5.4 *Monitoring Circulating Fluorescent Microspheres and Fluorescence-Labeled Cells In Vivo*

To demonstrate the ability to perform multicolor detection of circulating fluorescent particles *in vivo*, fluorescent microspheres or fluorescence-labeled cells were injected through the tail vein of a mouse. Two-photon flow cytometry measurements were performed at a blood vessel in the mouse ear. Before the injection of the fluorescent microspheres or the DeepRed-labeled splenocytes, the background signals in both S channel and L channels were recorded with the femtosecond NIR laser beam focused in various locations within the mouse ear. The measured background control traces before each injection are shown to the left of the orange line in Figs. 12(a) and 12(d). The thresholds were adjusted so that no peaks exist in the control traces. The amount of autofluorescence noise, which accounts for a large portion of the background, comes from the tissue at the focus of the laser beam. With translocation of the laser focus, a much higher autofluorescence signal is observed from blood vessel wall than from the blood itself. The sudden increase of background in Fig. 12(d) toward the end of the trace can thus be explained by a shift in the mouse ear. The background in the S channel of the mouse injected with DeepRed-labeled cells [Fig. 12(e)] was higher than that injected with fluorescence microspheres [Fig. 12(b)]. This can also be explained by the different site of laser focus in the mouse ear for the two experiments. In addition, the S channel background in Fig. 12(d) changed dramatically for the data taken 2 h and 1 day after the initial injection. This can be attributed to the tremble of the anesthetized mouse during data acquisition. In spite of this, the background fluorescence in the L channel remains at a low level throughout the whole experiments, allowing fluorescent peaks to be selected.

Figure 12(a) shows the S and L channel traces of a mouse injected with the 2.0-μm yellow-green fluorescent microspheres, in which a peak in the S channel corresponds to a microsphere passing through the excitation region [Fig. 12(b)]. Figure 12(d) shows the two-channel traces of a mouse injected with DeepRed-labeled splenocytes, in which a peak in the L channel corresponds to a cell [Fig. 12(e)]. Thus, circulating 2.0-μm yellow-green fluorescent microspheres and DeepRed-labeled splenocytes were detected in short and long spectral detection channels, respectively. The two-channel detection method enables differentiation of different cell or particles based on the fluorescence wavelength. It is also possible to conduct two-channel ratiometric measurements *in vivo*, as demonstrated previously *in vitro*. In this particular experiment, however, direct ratiometric measurements would not have been possible, since different individuals were used for DeepRed-labeled splenocytes or fluorescent microspheres, and thus the dissimilar spatial distributions of the the two fluorescent species is of no consequence.

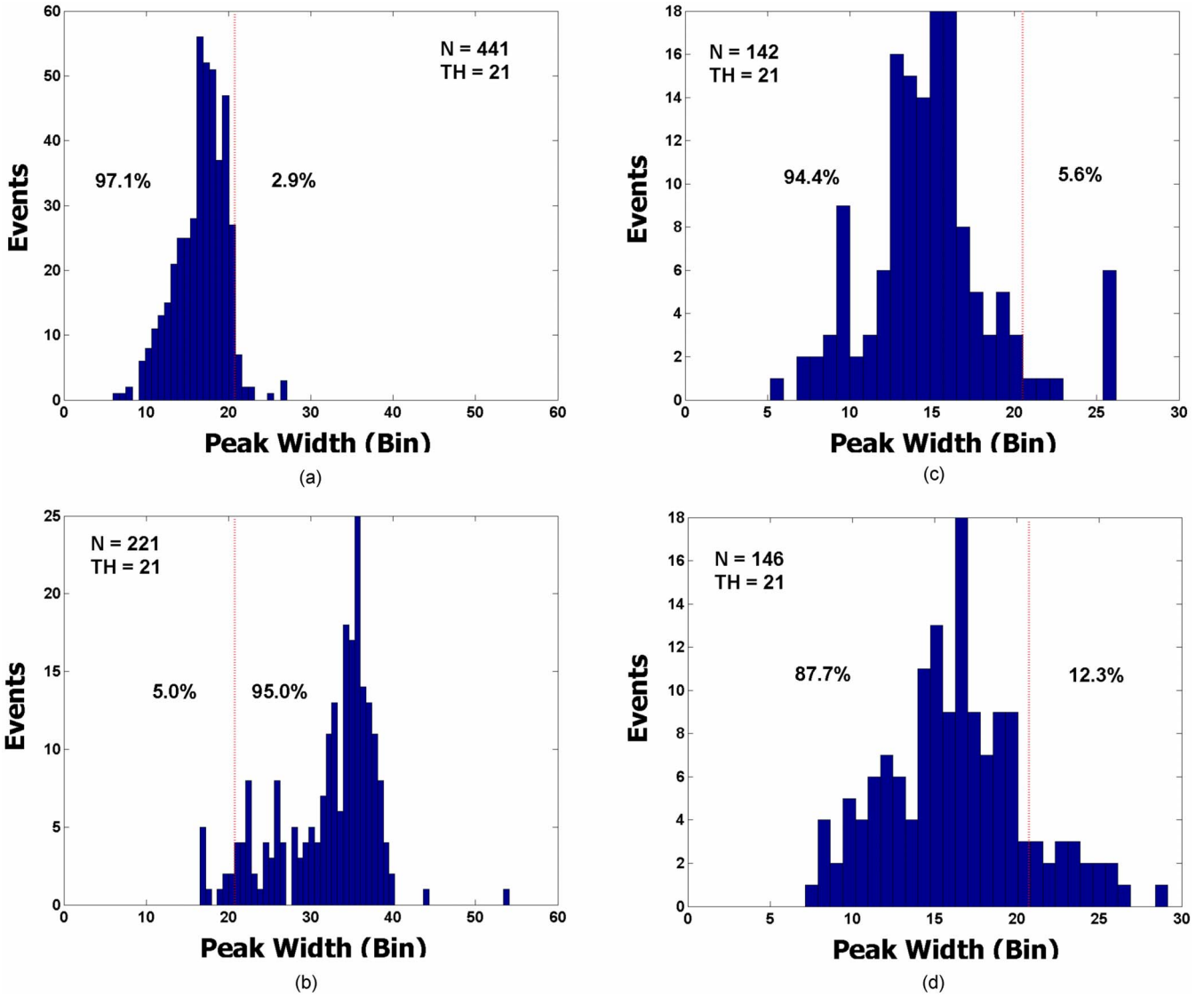

Fig. 11 Aggregation measurements made using T^3FC with the peak width distribution of (a) 6-μm fluorescent microspheres, (b) 10-μm fluorescent microspheres, (c) Jurkat cells stained with CFSE, and (d) aggregated (induced by ConA) Jurkat cells stained with CFSE. Thresholds for differentiating aggregates or large particles from individual small particles are marked as orange dashed lines. (Color online only.)

The double-peak event in Fig. 12(b) is probably the fluorescent trace of clogged fluorescent microspheres. For the fluorescent microspheres, about 20% of the detected events contained double peaks. For DeepRed-labeled splenocytes, almost no large peaks were observed. A double-peak event is treated as a single event if the fluorescent signal between the two peaks does not fall below the background threshold value.

5.5 *The Dynamics of Circulating Fluorescent Microspheres and Fluorescence-Labeled Cells*

The number of detected fluorescent microspheres and DeepRed-labeled splenocytes at different time points is shown in Figs. 12(c) and 12(f), respectively. For both of experiments, fluorescent microspheres or DeepRed-labeled cells were detected in the ear blood vessel immediately after tail vein injection (less than 30 s delay), which was indicated by the sudden increases in frequency of events. The frequency dropped to less than 10% within the first 10 to 20 min. The frequency went up again with reinjection of the same amount of fluorescent microspheres or DeepRed-labeled splenocytes. Similar depletion dynamics were observed. The experiments were repeated at the same location in the mouse ear 2 h and 1 day after the initial injection. No fluorescent microspheres were observed (not show here), while a few circulating DeepRed-labeled splenocytes were detected.

The depletion dynamics of circulating fluorescent microspheres in CD-1 mice and DeepRed-labeled splenocytes in NU/NU CD-1 mice using the *in vivo* two-photon flow cytometer and conventional flow cytometer is shown in Fig. 13. For the CD-1 mouse injected with fluorescent microspheres, the S channel traces after the first and second injection were used to calculate the frequency of detected events [Fig. 13(a)]. For the NU/NU CD-1 mouse injected with DeepRed-labeled splenocytes, the L channel trace after the first injection was used [Fig. 13(c)]. The frequency was calculated as the number of

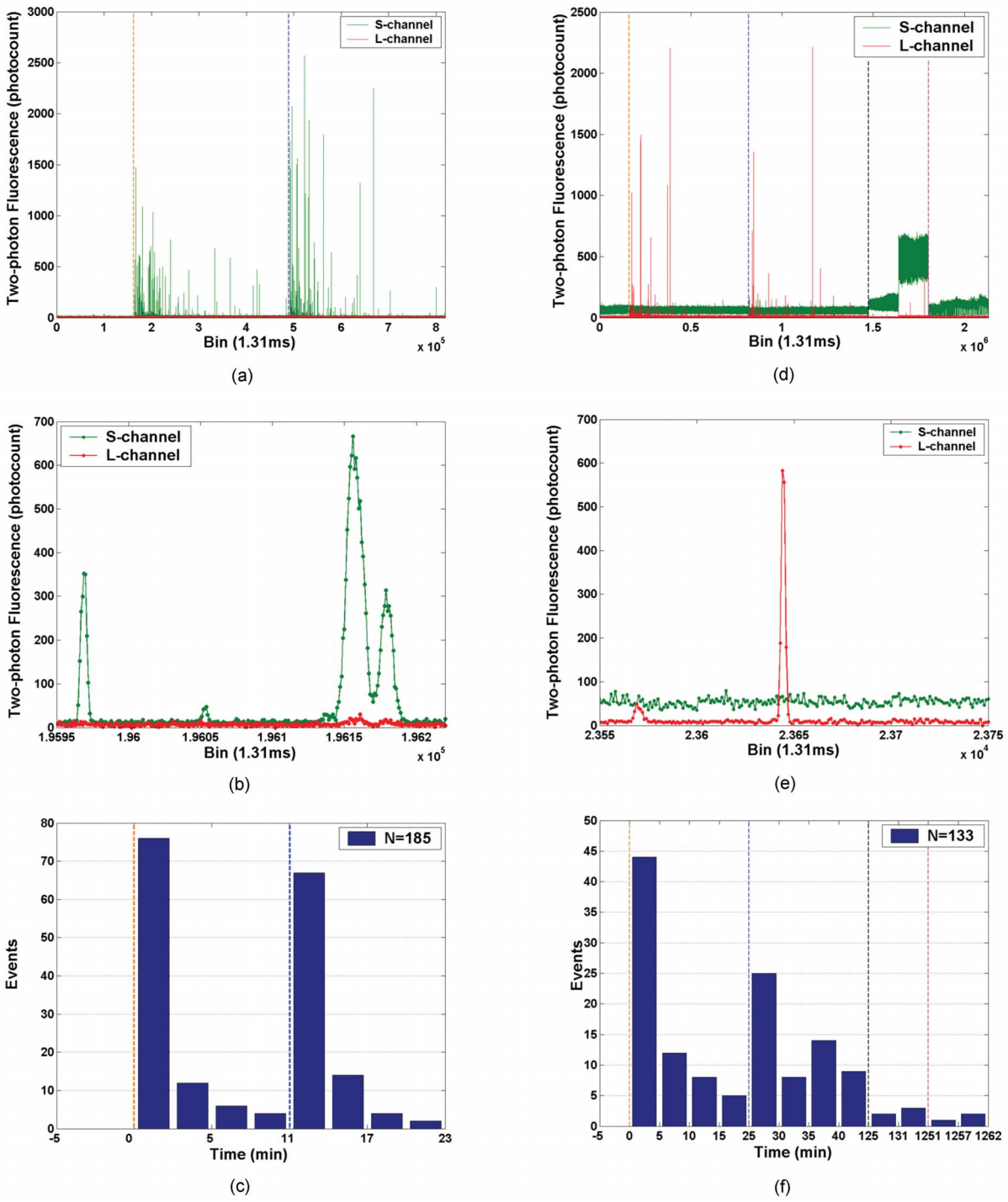

Fig. 12 (a) S channel (green) and L channel (red) traces from an ear blood vessel of a CD-1 mouse injected with 2.3×10^9 yellow-green fluorescent (Ex505/Em515) 2.0-μm microspheres at time zero and 11 min after. The control traces are shown to the left of the orange dashed line. The orange and blue dashed lines corresponds to the first and second injection, respectively. Each spike in the S channel corresponds to the fluorescent burst from microspheres passing through the excitation region. (b) Blow up of the dual-channel raw data showing detail of individual fluorescent peaks. (c) Number of detected events at different time points before and after injection. Each time point is represented by number of peaks above the background threshold during a period of 107 s. (d) S channel (green) and L channel (red) traces from an ear blood vessel of a NU/NU CD-1 mouse injected with 3.6×10^6 DeepRed-labeled splenocytes at time zero and 25 min after. The control traces are shown to the left of the orange dashed line. The orange, blue, black, and magenta dashed lines correspond to the first injection, the second injection, 2 h after initial injection, and 1 day after, respectively. Each spike in the L channel corresponds to the fluorescent burst from DeepRed-labeled splenocytes passing through the excitation region. (e) Magnified dual-channel raw data. (f) Number of detected events at different time points before and after injection. Each time point is represented by the number of peaks above the background threshold during a period of 214 s. (Color online only.)

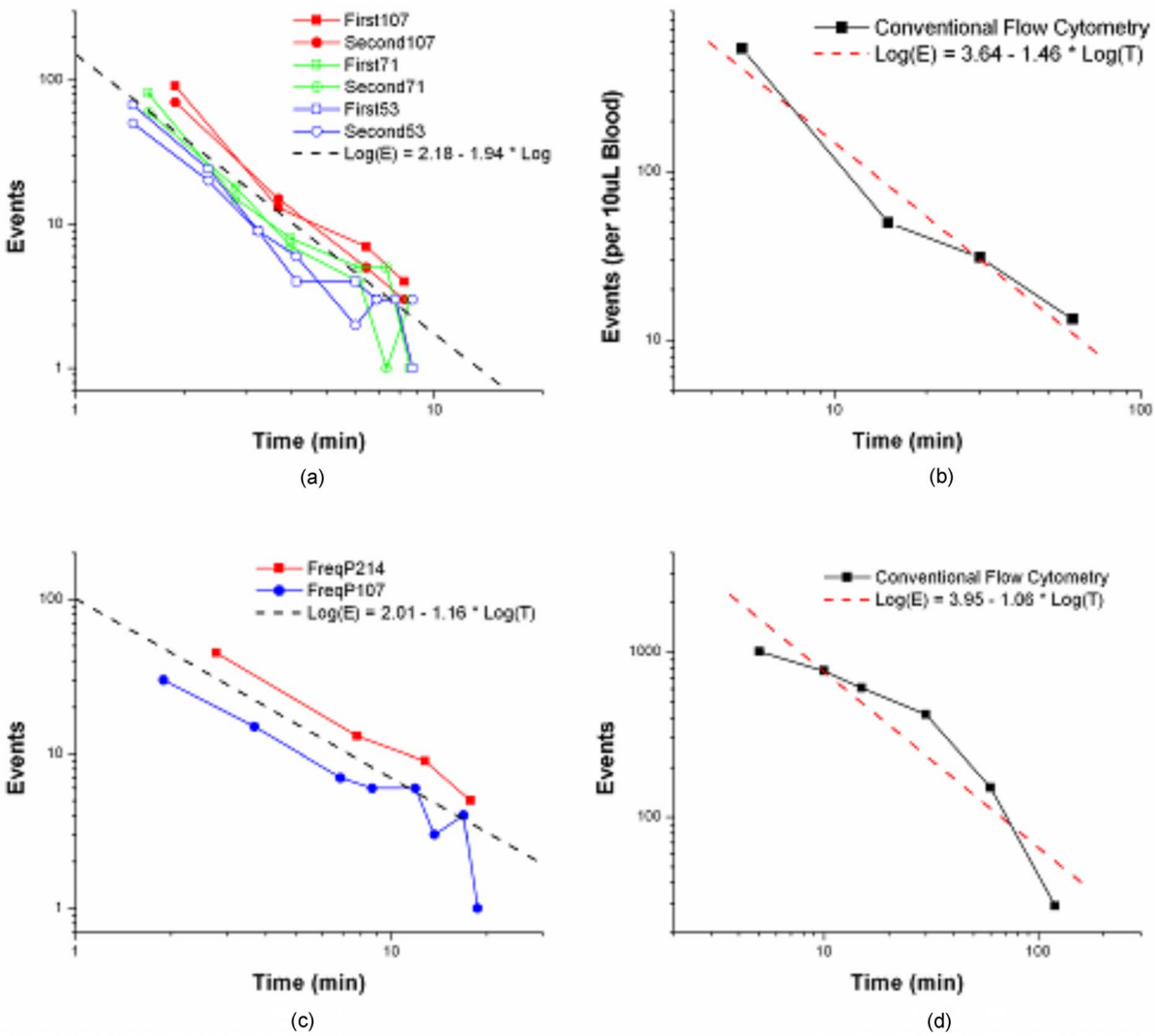

Fig. 13 Depletion dynamics of circulating fluorescent microspheres or cells. (a) The 10-min frequency dynamics in the blood vessel of a CD-1 mouse after the first (square marker) and the second (round marker) injection of 2.3×10^9 yellow-green fluorescent 2.0-μm microspheres. The frequency was calculated as the number of peaks in the S channel within 107 s (red), 71 s (green), or 53 s (blue). Both axes are in log scale. The coefficient of the linear fit (black dashed line) is the average of the coefficients from all six decay curves. (b) Frequency dynamics obtained by *ex vivo* analysis using a conventional flow cytometer. Blood was drawn at different time points from the mouse after injection of the same dose of microsphere solution. A linear fit is obtained (red dashed line) in the log-log plot. (c) The 20-min frequency dynamics in the blood vessel of a NU/NU CD-1 mouse after the first injection of 3.6×10^6 DeepRed-labeled splenocytes. The frequency was calculated as the number of peaks in the L channel within 214 (red) or 107 s (blue). Both axes are on a log scale. The coefficient of the linear fit (black dashed line) is the average of the coefficients from both of the decay curves. (d) Frequency dynamics obtained by *ex vivo* analysis using a conventional flow cytometer. Blood was drawn at different time points from the mouse after injection of the same dose of DeepRed-labeled splenocytes. A linear fit is obtained (red dashed line) on the log-log plot. (Color online only).

events within a certain time period. The time points beyond 10 or 20 min were not used to generate the fitting, as the number of detected cells fell below 1 event/min. The number of fluorescent microspheres [Fig. 13(b)] or CFSE-labeled splenocytes [Fig. 13(d)] in 10 μL of blood drawn at different time points after injection was detected *ex vivo* using a conventional flow cytometer. Blood samples are not able to be drawn rapidly enough from the mouse for conventional flow cytometry to follow the depletion dynamics over the course of a few minutes as accurately as the *in vivo* flow cytometer enables.

The *in vivo* flow cytometry results show that the fluorescent microspheres deplete faster in the circulation of a CD-1 mouse than fluorescence-labeled splenocytes in NU/NU CD-1 mouse. The average slope coefficients are −1.94 and −1.16 for circulating fluorescent microspheres and DeepRed-labeled splenocytes, repectively. This difference in depletion rate was also observed from the *ex vivo* flow cytometry results, where the slope coefficients are −1.46 and −1.06 for circulating fluorescent microspheres and CFSE-labeled splenocytes, repectively. The reasons for the frequency drop could be that the microbeads or splenocytes clogged in the blood stream, stuck to the blood vessel surfaces, were removed by lysis or phagocytosis, or were filtered by organs in the circulation.

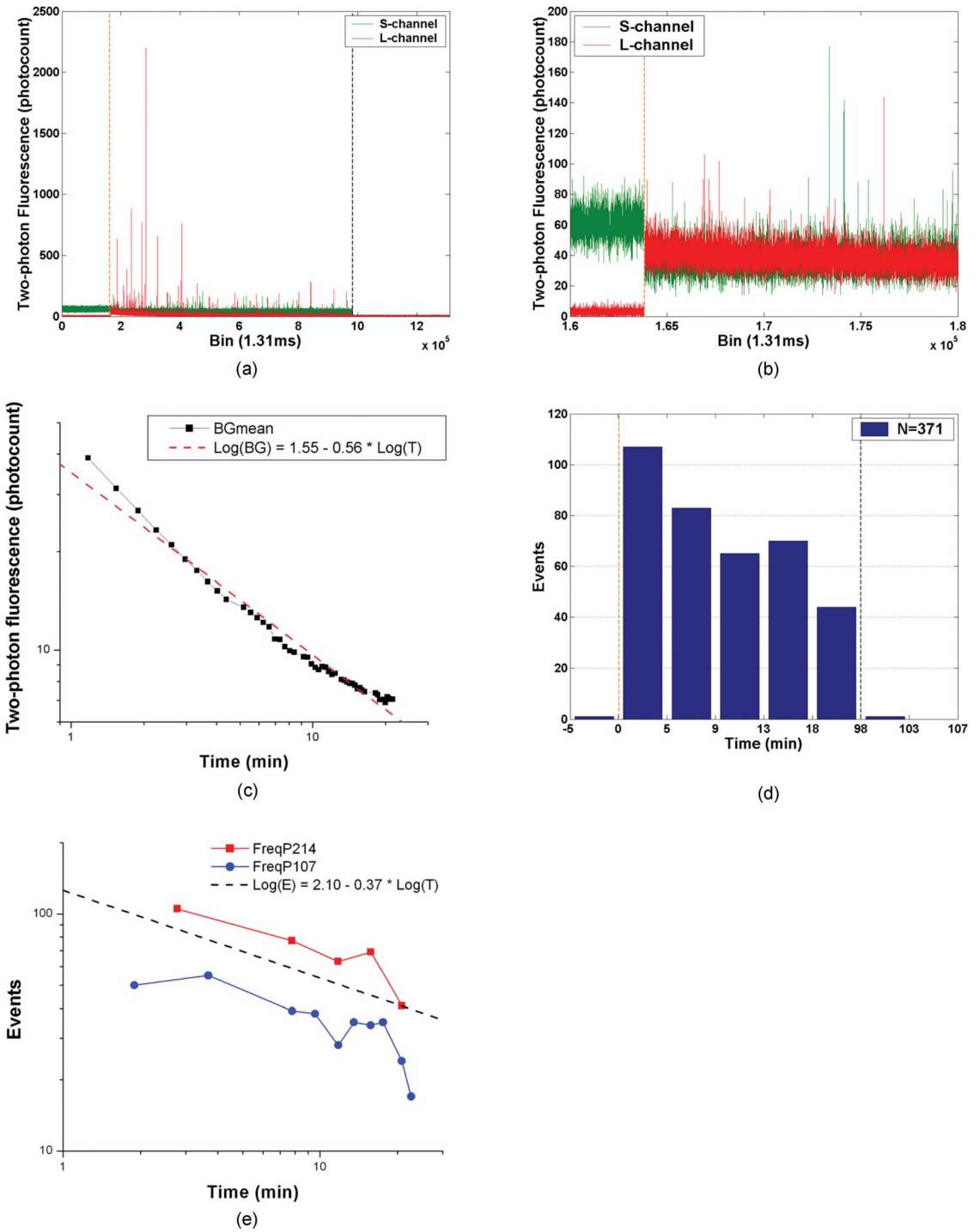

Fig. 14 (a) S channel (green) and L channel (red) traces from a blood vessel in the ear of a NU/NU CD-1 mouse injected with 300 μL (5 μM) DeepRed solution at time zero. The control traces are shown to the left of the orange dashed line. The orange and black dashed lines correspond to the initial injection and 1.5 h after initial injection, respectively. Each spike in the L channel corresponds to the fluorescent burst from DeepRed fluorophores in cells passing through the excitation region. (b) Magnified dual-channel raw data at the time of injection showing the background rise in the L channel after injection of free DeepRed dye solution. Individual fluorescent peaks above the background noise can also be observed in the L channel after the injection of the free DeepRed dye solution. (c) The background two-photon excited fluorescent signal in the L channel at different time points after the injection of DeepRed dye solution. The fluorescent peaks above threshold were not counted in the background signal. The red dashed line is the linear fit of the log value of two-photon fluorescence against time. (d) Number of detected events at different time points before and after injection. Each time point is represented by the number of peaks above the background threshold during a period of 214 seconds. (e) The 20-min peak frequency dynamics in the blood vessel of a NU/NU CD-1 mouse after the injection of 300 μL of DeepRed solution. The frequency was calculated as the number of peaks in the L channel within 214 (red) or 107 s (blue) time duration. Both axes are on a log scale. The coefficient of the linear fit (black dashed line) is the average of the coefficients from both of the decay curves. (Color online only.)

The different depletion rates indicate the circulation time of splenocytes in an immmunodeficient NU/NU CD-1 mouse is longer than that of fluorescent microspheres in a CD-1 mouse.

For both circulating fluorescent microspheres and fluorescence-labeled splenocytes, the depletion rate in the first 10 min after injection obtained by *in vivo* flow cytometry is larger than the rate in the first 1.5 h obtained by *ex vivo* flow cytometry analysis. The difference of the depletion rates from *in vivo* and *ex vivo* measurements could be attributed to the different time scales in the depletion process. It could also be the systematic error in the *ex vivo* method introduced by the significant delay between blood withdrawal and flow cytometry analysis.

According to previous results,[24,32] one challenge to doing *in vivo* cytometry is the small number of labeled cells at the detection region relative to the number injected into the animal. To have a statistically significant result, a larger number of cells must be detected. One solution would be to access larger blood vessels with higher blood flow rates. A femtosecond NIR laser source has the advantage of being able to penetrate much deeper through biological tissue than a one-photon cw laser,[33] though it is in fact not always the case that larger vessels are deeper, a notable counterexample being the brain. In addition, the nonlinear excitation property of a femtosecond NIR laser confines the excitation region to appear only at the focus without using a confocal pinhole. This reduces photodamage to the surrounding biological tissue, which may extend the monitoring time in live animals.

5.6 *Monitoring Fluorescent Dye Staining Process In Vivo*

The two-channel fluorescence traces from an ear blood vessel were monitored as free DeepRed dye solution was injected through the tail vein [Fig. 14(a)]. As shown in [Fig. 14(b)], the background signal in the long channel rose immediately after the injection, due to the presence of the DeepRed fluorophores in the mouse blood. After the injection, the background signal gradually decreased, as the dye molecules permeated through the blood vessel walls or were filtered out of the circulation. The average background signal at different time points is ploted against time in a log scale [Fig. 14(c)], and a linear fit of the signal decay reveals a slope coefficient of −0.56. Compared with the depletion rate of fluorescent microspheres or fluorescence-labeled splenocytes, the background decay rate is much slower.

The peaks above the background were also observed in the L channel trace signal. DeepRed is a cell-permeating probe that binds to the outer membrane of mitochondria in living cells and measures their viability. As the DeepRed dye solution circulates in the vasculature, it labels the circulating lymphocytes. Therefore, the peaks should correspond to the *in vivo* labeled cells passing through the two-photon excitation region. The number of peaks above threshold at different time points was acquired [Fig. 14(d)]. The threshold was adjusted according to the gradually changing background fluorescence signal. The frequency of *in vivo* labeled cells decreases after the injection, with the exception of the 15-min data point, which could be accounted for, for example, by an increase in blood flow with change in mouse temperature. An average depletion rate of −0.37 was obtained by fitting the number of detected events in the first 20 min after injection [Fig. 14(e)]. This rate is much slower than the those of fluorescent microspheres or fluorescence-labeled splenocytes shown previously. One and half hours after the initial injection of free DeepRed dye, only one event was observed in a 6-min interval.

6 Conclusion

We have demonstrated a novel technique to do cytometry: two-photon excitation to selectively detect single cells; two-dye labeling with two-channel detection to normalize nonuniform excitation; two-beam scanning to normalize flow parameters for particle size measurements in unregulated flow. Experiments performed both *in vitro* in the modeling glass capillary and *in vivo* on live mice showed that quantitative flow cytometric measurement is possible in greatly simplified flow systems with appropriate trigger and reporter dye labeling, such as the receptor-mediated uptake of targeted fluorescent-labeled nanoparticles to tackle the nonhomogenous cellular distribution of two dyes. This novel two-photon flow cytometer opens up a wide range of new applications, such as direct *in vivo* measurements in circulating blood, as well as *in vitro* measurements in highly simplified and compact microfluidics systems.[34,35]

Although enumeration of circulating cells *in vivo* has been achieved with confocal detection using one-photon excitation,[36] the two-photon flow cytometry technique offers potential advantages for *in vivo* cytometric measurements. Under nonuniform flow, uneven excitation presents a serious challenge to quantifying single cell events. Fluorescence intensity alone is not a good measure for cellular properties, as the intensity is affected by the uneven excitation. The two-channel ratiometric method provides a solution to quantify the fluorescence from labeled cells *in vivo* in spite of the flow condition. To perform the ratiometric measurement using confocal one-photon excitation, multiple lasers are required to excite different dyes, which have distinct one-photon absorption spectra. The optical layout can rapidly become complex. On the other hand, a single femtosecond NIR laser source may be used to excite a wide variety of fluorophores. The large separation between the NIR excitation and the visible fluorescence wavelength makes it easier to attenuate scattered excitation light while collecting the entire fluorescence spectrum with high efficiency.[37] Thus, using a NIR femtosecond laser as the excitation source for cytometry allows ratiometric measurements through simplified optical filtering and fluorescence background reduction.

Acknowledgments

This project has been funded in whole or in part with federal funds from the National Aeronautics and Space Administration (NASA) Ames Research Center, under Contract No. NAS2-02069.

References

1. F. Helmchen and W. Denk, "Deep tissue two-photon microscopy," *Nat. Methods* **2**, 932–940 (2005).
2. A. Diaspro, G. Chirico, and M. Collini, "Two-photon fluorescence excitation and related techniques in biological microscopy," *Q. Rev. Biophys.* **38**, 97–166 (2005).

3. P. Hänninen, J. Soini, and E. Soini, "Photon-burst analysis in two-photon fluorescence excitation flow cytometry," *Cytometry* **36**, 183–188 (1999).
4. A. Diaspro, "Two-photon excitation. A new potential perspective in flow cytometry," *Minerva Biotecnol.* **11**, 87–92 (1999).
5. W. He, H. Wang, L. Hartmann, J. Chen, and P. Low, "*In vivo* quantiation of rare circulating tumor cells by multiphoton intravital flow cytometry," *Proc. Natl. Acad. Sci. U.S.A.* **104**, 11760–11765 (2007).
6. H. M. Shapiro, *Practical Flow Cytometry*, Wiley-Liss, New York (2003).
7. M. G. Ormerod, *Flow Cytometry*, Springer-Verlag, New York (1999).
8. M. A. Van Dilla, T. T. Trujillo, P. F. Mullaney, and J. R. Coulter, "Cell microfluorometry: a method for rapid fluorescence measurements," *Science* **163**, 1213–1214 (1969).
9. R. Miyake, H. Ohki, I. Yamazaki, and R. Yabe, "A development of micro sheath flow chambers," in *Proc. the IEEE Micro Electro Mechanical Systems Workshop*, p. 265–270, Nara, Japan (1991).
10. D. Sobek, S. D. Senturia, and M. L. Gray, "Microfabricated fused silica flow chambers for flow cytometry, in *Proc. Solid-State Sensor and Actuator Workshop*, p. 260–263, Hilton Head, SC (1994).
11. U. D. Larsen, G. Blankenstein, and J. Branebjerg, "Microchip Coulter particle counter," in *Proc. the Int. Conf. on Solid-State Sensors and Actuators, TRANSDUCERS '97*, Vol. **2**, p. 1319–1322, Chicago (1997).
12. M. Koch, A. G. R. Evans, and A. Brunnschweiler, "Design and fabrication of a micromachined Coulter counter," *J. Micromech. Microeng.* **9**, 159–161 (1999).
13. D. Huh, Y. C. Tung, H. H. Wei, J. B. Grotberg, S. J. Skerlos, K. Kurabayashi, and S. Takayama, "Use of air-liquid two-phase flow in hydrophobic microfluidic channels for disposable flow cytometers," *Biomed. Microdevices* **4**, 141–149 (2002).
14. P. J. Crosland-Taylor, "A device for counting small particles suspended in a fluid through a tube," *Nature (London)* **171**, 37–38 (1953).
15. A. Y. Fu, C. Spence, A. Scherer, F. H. Arnold, and S. R. Quake, "A microfabricated fluorescence-activated cell sorter," *Nat. Biotechnol.* **17**, 1109–1111 (1999).
16. J. Condeelis and J. E. Segall, "Intravital imaging of cell movement in tumours," *Nat. Rev. Cancer* **3**, 921–930 (2003).
17. E. Chaigneau, M. Oheim, E. Audinat, and S. Charpak, "Two-photon imaging of capillary blood flow in olfactory bulb glomeruli," *Proc. Natl. Acad. Sci. U.S.A.* **100**, 13081–13086 (2003).
18. M. J. Miller, S. H. Wei, I. Parker, and M. D. Cahalan, "Two-photon imaging of lymphocyte motility and antigen response in intact lymph node," *Science* **296**, 1869–1873 (2002).
19. M. D. Cahalan, I. Parker, S. H. Wei, and M. J. Miller, "Two-photon tissue imaging: seeing the immune system in a fresh light," *Nat. Rev. Immun.* **2**, 872–880 (2002).
20. E. Yoder, "*In vivo* microscopy of the mouse brain using multiphoton laser scanning techniques," *Prog. Biomed. Opt. Imaging* **3**, 14–29 (2002).
21. C. F. Zhong, J. Y. Ye, A. Myc, T. P. Thomas, A. U. Bielinska, J. R. Baker, Jr., and T. B. Norris, "Two-photon flow cytometry," *Proc. SPIE* **5700**, 78–89 (2005).
22. C. F. Zhong, J. Y. Ye, A. Myc, Z. Cao, J. Kukowska, J. R. Baker, Jr., and T. B. Norris, "*In vivo* flow cytometry," in *Proc. OSA FiO/LS Meeting*, OSA (2004).
23. C. F. Zhong, P. T. Thommey, J. Y. Ye, A. Myc, A. Bielinska, J. R. Baker, Jr., and T. B. Norris, "Quantitative two-photon flow cytometry," in *Proc. CLEO/QELS and PhAST 2005*, OSA (2005).
24. C. F. Zhong, P. T. Thommey, J. Y. Ye, Z. Cao, A. Myc, J. R. Baker, Jr., and T. B. Norris, "Multiphoton *in vivo* flow cytometry," in *Proc. CLEO/QELS and PhAST 2005*, OSA (2005).
25. E. R. Tkaczyk, C. F. Zhong, J. Y. Ye, A. Myc, T. Thomas, Z. Cao, R. Duran-Struuck, K. E. Luker, G. D. Luker, J. R. Baker, and T. B. Norris, "Two-photon, two-color *in vivo* flow cytometry to noninvasively monitor multiple circulating cell lines," *Proc. SPIE* **6631**, 663107 (2007).
26. E. R. Tkaczyk, C. F. Zhong, J. Y. Ye, A. Myc, T. Thomas, Z. Cao, R. Duran-Struuck, K. E. Luker, G. D. Luker, T. B. Norris, and J. R. Baker, "*In vivo* monitoring of multiple circulating cell Populations using two-photon flow cytometry," *Opt. Commun.* **281**, 888–894 (2008).
27. E. R. Tkaczyk, J. Y. Ye, A. Myc, S. Katnik, K. E. Luker, G. D. Luker, J. R. Baker, and T. B. Norris, "*In vivo* extended cavity laser enhanced two-photon flow cytometry," *J. Biomed. Opt.* **13** (2008) (in press)
28. J. E. Gestwicki, L. E. Strong, C. W. Cairo, F. J. Boehm, and L. L. Kiessling, "Cell aggregation by scaffolded receptor clusters," *Chem. Biol.* **9**, 163–169 (2002).
29. D. Mazza, F. Cella, G. Vicidomini, S. Krol, and A. Diaspro, "Role of three-dimensional bleach distribution in confocal and two-photon fluorescence recovery after photobleaching experiments," *Appl. Opt.*. **46**, 7401–7411 (2007).
30. A. Nagy, J. Wu, and K. M. Berland, "Characterizing observation volumes and the role of excitation saturation in one-photon fluorescence fluctuation spectroscopy," *J. Biomed. Opt.* **10**, 044015 (2005).
31. T. P. Thomas, M. T. Myaing, J. Y. Ye, K. Candido, A. Kotlyar, J. Beals, P. Cao, B. Keszler, A. K. Patri, T. B. Norris, and J. R. Baker, "Detection and analysis of tumor fluorescence using a two-Photon optical fiber probe," *Biophys. J.* **86**, 3959–3965 (2004).
32. I. Georgakoudi, N. Solban, J. Novak, W. L. Rice, X. B. Wei, T. Hasan, and, C. P. Lin, "*In vivo* flow cytometry: a new method for enumerating circulating cancer cells," *Cancer Res.* **64**, 5044–5047 (2004).
33. M. Gu, X. S. Gan, A. Kisteman, and M. G. Xu, "Comparison of penetration depth between two-photon excitation and single-photon excitation in imaging through turbid tissue media," *Appl. Phys. Lett.* **77**, 1551–1553 (2000).
34. M. Foquet, J. Korlach, W. Zipfel, W. W. Webb, and H. G. Craighead, "DNA fragment sizing by single molecule detection in submicrometer-sized closed fluidic channels," *Anal. Chem.* **74**, 1415–1422 (2002).
35. A. Y. Fu, C. Spence, A. Scherer, F. H. Arnold, and S. R. Quake, "A microfabricated fluorescence-activated cell sorter," *Nat. Biotechnol.* **17**, 1109–1111 (1999).
36. J. Novak, I. Georgakoudi, X. Wei, A. Prossin, and C. P. Lin, "*In vivo* flow cytometer for real-time detection and quantification of circulating cells," *Opt. Lett.* **29**, 77–79 (2004).
37. K. Konig, "Multiphoton microscopy in life sciences," *J. Microsc.* **200**, 83–104 (2000).